ISTANBUL TECHNICAL UNIVERSITY ★ GRADUATE SCHOOL OF SCIENCE
ENGINEERING AND TECHNOLOGY

Maximum Power Point Tracking in Photovoltaic Panels with Particle Swarm Optimization Algorithm

M.Sc. THESIS

Mohammadreza ESMALI NOJEHDEH

Electrical Engineering Department

Electrical Engineering Programme

May 2015

ISTANBUL TECHNICAL UNIVERSITY ★ GRADUATE SCHOOL OF SCIENCE
ENGINEERING AND TECHNOLOGY

Maximum Power Point Tracking in Photovoltaic Panels with Particle Swarm Optimization Algorithm

M.Sc. THESIS

Mohammadreza ESMALI NOJEHDEH
(504111058)

Electrical Engineering Department

Electrical Engineering Programme

Thesis Advisor: Asst. Prof. Dr. Deniz YILDIRIM

May 2015

İSTANBUL TEKNİK ÜNİVERSİTESİ ★ FEN BİLİMLERİ ENSTİTÜSÜ

Güneş Panellerinde Parçacık Sürü Optimizasyonu ile Maksimum Güç Takibi

YÜKSEK LİSANS TEZİ

Mohammadreza ESMALI NOJEHDEH
(504111058)

Elektrik Mühendisliği Anabilim Dalı

Elektrik Mühendisliği Programı

Tez Danışmanı: Asst. Prof. Dr. Deniz YILDIRIM

Mayıs 2015

Mohammadreza ESMALI NOJEHDEH, a M.Sc. student of ITU Graduate School of Science Engineering and Technology 504111058 successfully defended the thesis entitled **"Maximum Power Point Tracking in Photovoltaic Panels with Particle Swarm Optimization Algorithm"**, which he/she prepared after fulfilling the requirements specified in the associated legislations, before the jury whose signatures are below.

Thesis Advisor : **Asst. Prof. Dr. Deniz YILDIRIM** ....
Istanbul Technical University

Jury Members : **Assoc. Prof. Dr. Önder GÜLER** ....
Istanbul Technical University

Asst. Prof. Dr. Murat YILMAZ ....
Istanbul Technical University

Date of Submission : **4 May 2015**
Date of Defense : **27 May 2015**

To my parents,

FOREWORD

This Master thesis has been completed also thanks to many persons which contributed with suggestions, thoughts, and constructive criticisms.
I would like to thank my supervisor Dr.Deniz YILDIRIM for giving me valuable advice and support always when needed. My thanks to all members of the jury of the thesis dissertation.
Last but not least, thanks a lot to my family, for always supporting me during my studies abroad.

May 2015

Mohammadreza ESMALI NOJEHDEH
(Electrical Engineer)

TABLE OF CONTENTS

Page

ABBREVIATIONS

PSO	: Particle Swarm Optimization
MPPT	: Maximum Power Point Tracking
MPP	: Maximum Power Point
P&O	: Perturb and Observe
DSP	: Digital Signal Processor
PV	: Photovoltaics
RCC	: Ripple Correlation Control
PI	: Proportional-Integral
OCC	: One-Cycle Control
BFV	: Best Fixed Voltage
LRCM	: Linear Reoriented Coordinates Method
AD	: Analog to Digital
STC	: Standard Test Condition

LIST OF TABLES

LIST OF FIGURES

Page

LIST OF SYMBOLS

t	:	time
T	:	temperature
P	:	power
V	:	voltage
I	:	current
e	:	error signal
k_1	:	constant of proportionality
k_2	:	constant of proportionality
k_3	:	constant of proportionality
d	:	duty ratio
k_4	:	proportionality constant
τ	:	time constant
u	:	switch function
R	:	resistance
k	:	boltzman constant
q	:	electron charge
m	:	ideal factor of diode
v_t	:	thermal voltage
e	:	neper constant
FF	:	fill factor
FF_0	:	ideal fill factor
G	:	irradiance
D	:	duty cycle
L	:	inductor
C	:	capacitor
$M(D)$	:	conversion ratio
f	:	frequency
$\dot{p}$	:	time derivative of power
$\dot{i}$	:	time derivative of current
$\dot{v}$	:	time derivative of voltage
α	:	current sweep parameter
β	:	voltage sweep parameter

Maximum Power Point Tracking in Photovoltaic Panels
with Particle Swarm Optimization Algorithm

SUMMARY

Studies on photovoltaic systems are increasing because of a large, secure, essentially exhaustible and broadly available resource as a future energy supply. However, the output power induced in the photovoltaic modules is influenced by an intensity of solar cell radiation, temperature of the solar cells and so on. Therefore, to maximize the efficiency of the renewable energy system, it is necessary to track the maximum power point of the input source. Particle swarm optimization (PSO) technique is used to identify the optimal power point of a photovoltaic module used in a stand-alone (PV) system.

The PSO algorithm searches the maximum power point of the PV module by determining the array power at maximum point. The tracked variable is used as a reference value (set point) to an ON/OFF controller of a dc boost chopper such that the PV module is forced to operate at the optimal power point. In this thesis the controller is ATmega32 by ATMEL©.

This microcontroller by measuring voltage and current of panel and changing duty cycle ON/OFF switch of boost converter, and via PSO algorithm cause panel operate on maximum power point.

The advantage of this method versus of other method which use microcontroller like look table-up method, this method does not need any information about panel and environment condition i.e, we can use this controller for any panel in any condition also changing of temperature and irradiation does not affect operation.

This method does not need any control loop so it is low cost, which does process with AVR microcontroller and current sensor. By comparing this algorithm with other intelligent systems like fuzzy controller or neural network system this algorithm is more simple.

Güneş Panellerinde Parçacık Sürü Optimizasyonu ile Maksimum Güç Takibi

ÖZET

Son yıllarda özellikle fosil yakıtların çevreye olan zararları ve bu tür enerji kaynaklarının gittikçe azalmasıyla beraber, küresel ısınma ve iklim değişiklikleri sebebiyle temiz enerji kaynaklarına duyulan gereksinim giderek artmıştır. Yerkürede bulunduğu konum açısından güneşlenme alanı ve süresi oldukça iyi olan Türkiye'de güneş enerjisi alternatif enerji kaynağı olarak öne çıkmaktadır. Bu açıdan bakıldığında güneş enerjisi gelecek yıllar için yerli enerji kullanımının yaygınlaşması açısından önemli bir alternatif enerji kaynağı olarak karşımıza çıkmaktadır.

Fotovoltaik sistemler üzerine olan çalışmalar, güneş enerjisinin büyük, güvenli, hiç bitmeyen ve dünyanın her yerinde erişebilen bir enerji kaynağı olması nedeniyle artmaktadır. Güneş enerjisini elektrik enerjisine dönüştüren elemanlar güneş panelleri veya fotovoltaik piller olarak adlandırılmaktadır. Güneş enerjisi kullanımının birçok avantajına karşılık güneş panellerinin kurulum maliyetlerinin oldukça yüksek ve kendilerini amorti edebilme süreleri ise oldukça uzundur. Bu sebepten dolayı son zamanlarda mevcut panellerden en iyi şekilde yararlanmak ve en yüksek verimi elde edebilmek amacıyla yeni çalışmalar yapılmaktadır.

Bununla beraber, fotovoltaik modüllerden elde edilen çıkış gücü hücre üzerine düşen ışınımın şiddeti, hücre sıcaklığı ve benzeri durumlardan etkilenmektedir. Bu nedenle, fotovoltaik sistemlerden elde edilen enerjinin maksimize edilebilmesi için, güneş hücrelerinin maksimum güç verdiği noktanın takip edilmesi gerekmektedir. Fotovoltaik panellerin maksimum verimle maksimum çıkış gücü sağlayarak çalıştığı maksimum güç noktası, güneş ışınlarının panel yüzeyine yaptığı açıya, güneşten yeryüzüne düşen ışınım değerine, panelin çıkışına bağlı olan yüke ve panel sıcaklığına bağlı olarak değişmektedir. Dolayısıyla panel çıkışına bağlanan herhangi bir yükün yer aldığı fotovoltaik sistemlerde çalışma noktası her zaman maksimum güç noktası değildir.

Beslenen yükün talep ettiği gücü sürekli olarak sağlayabilmek amacıyla fotovoltaik sistemler gerektiğinden daha fazla modül içerecek şekilde tasarlanırlar. Bu durumda sistem maliyeti oldukça yükselir, ayrıca önemli miktarda enerji kaybı yaşanır. Bu problemin çözümü için maksimum güç noktası izleyicisi (MGNİ) olarak adlandırılan anahtarlamalı güç konvertörü kullanılabilir. Böylece fotovoltaik panellerin maksimum güç noktasında sürekli çalışması sağlanarak optimum kullanımı mümkün olacaktır. MGNİ fotovoltaik panelin gerilim ve akımını yükten bağımsız olarak kontrol ederek bu işlemi gerçekleştirmektedir. Doğru tasarlanmış bir MGNİ algoritması ve modelleme hesaplamaları ile maksimum güç noktasının yeri ve bu değerin izlenmesi gerçekleştirilebilir.

Bu tezin amacı farklı ortam koşullarında değiştir ve izle yöntemini kullanarak fotovoltaik panelin maksimum güç noktasını takip etmektir. Bu hedefi başarmak

için bir doğru akım dönüştürücü ve kontrolör kullanılmaktadır. Çeviricinin çalışma oranını ayarlayan kontrolör gerçekte panelin çalışma gerilimini değiştirir. Bu tezde kullanılan Atmega32 mikrokontrolörü parçacık sürü optimizasyonu yöntemini kullanarak periyodik olarak maksimum güç noktasındaki gerilim değerini aramakta ve bu arama periyodu farklı ortam koşullarına bağlı olarak programlama ile kolayca değiştirilebilmektedir (bu tezde arama periyodu 10 saniye alınmıştır).

Sistemin çalışması için gerekli anahtarlama sinyalleri mikrokontrolör tarafından üretilmektedir. Aynı şekilde, dönüştürücünün girişindeki akım ve gerilim bilgileri mikrokontrolör tarafından okunarak sistemin gücü hesaplanmaktadır. Çalışmada, çıkış gücünün sürekli olarak en yüksek seviyede tutulması için "maksimum güç takibi" uygulaması geliştirilmiştir. Bu uygulama ile giriş gerilim seviyesindeki artış ya da azalmaya bağlı olarak, dönüştürücünün anahtarlama sinyalinin, iletim ve kesim oranları değiştirilmekte ve çıkış gerilimi hep maksimum gücü elde edecek şekilde ayarlanmaktadır. Kontrolörün ışınım ve yük değişimlerine karşı nasıl cevap vereceğinin de incelenmesi gerekmektedir çünkü ortam koşulları ışınım ve gölgelenme faktörleri tarafından hızlıca değişebilmektedir.

Bu tezin birinci kısmında panellerin maksimum güç noktasını takip etmek için kullanılan farklı yöntemler incelenmiş ve her yöntemin avantajları ve dezavantajları tartışılmıştır. Panel karakteristikleri, panelin matematiksel modeli ve eşdeğer devresi ikinci bölümde incelenmiştir.

Sistem konfigürasyonunun tartışıldığı üçüncü bölümde, yükseltici çeviricisi çalışma prensibi ve devre elemanlarının seçimi ile devre parametrelerinin hesabı yapılmıştır. Ayrıca maksimum güç noktasını takip etmek için kullanılan parçacık sürü optimizasyon algoritması açıklanarak, algoritmanın avantajı ve dezavantajları belirtilmiştir. Bu algoritmanın matematiksel modellenmesi ve algoritmanın çalışmasına etki eden önemli parametreler tartışılmıştır.

Simülasyon çalışmalarının yapıldığı dördüncü bölümde mikrokontrolör yazılımlarının da devre ile birlikte çalışmasına imkan veren bir program olması nedeniyle Proteus programı kullanılmıştır. Bu benzetim çalışmasında devrenin farklı senaryolardaki durumu incelenmiştir. İlk olarak sabit ortam koşullarında sistemin çalışması mikrokontrolörün nasıl maksimum güç noktasını elde edebileceği amacıyla test edilmiştir. Daha sonra sistem belli bir yük ile çalışırken, yük değişiminde sistem çalışması incelenmiştir. Yük değiştiği zaman eğer kontrolör yeni gerilim değerini takip edemezse çıkış güç değişecektir. Bir başka deyişle, aynı çıkış gücünü takip edebilmek için, kontrolör çalışma oranını değiştirmektedir. Son senaryoda ışınımın değişme durumu incelenmiştir. Bu durumda maksimum güç değeri ve çalışma gerilimi değişmektedir. Benzer şekilde kontrolörün maksimum güç noktasını takip etmesi için yeni bir çalışma oranı değeri bulması gerekmektedir.

Sistem prototipinin gerçeklendiği ve deneysel çalışmalarının yapıldığı son bölümde, devre elemanları belirtilmiş ve farklı çalışma senaryolarında prototip devrenin nasıl cevap verdiği incelenmiştir. Bu aşamada simülasyon çalışmalarında uygulanan senaryoların benzeri gerçek çalışma koşullarında prototip devreye uygulanmış ve bu iki sonuç arasında karşılaştırma yapılmıştır. Bu metodun mikrokontrolör ile önceden belirlenmiş değerlerin yer aldığı bir tabloya bakarak elde edilen değerlerini kullandığı diğer metoda göre avantajı, bu tezdeki yöntemde kullanılan kontrolörün herhangi bir panel ile veya herhangi bir çalışma koşulunda istenilen performansı verebilmelidir.

Sıcaklık ve ışınım gibi değerlerinin değişmesi güç noktasında bir değişikliğe sebep olduğunda, kontrolör otomatik olarak yeni güç değerini bulacaktır. Bu metod düşük maliyetli ve basit bir kontrol algoritması yapısına sahiptir. Bir gerilim ve bir akım sensörü kullanımı kontrolördeki algoritma için yeterlidir. Bu metodu bulanık kontrol veya yapay sinir ağı kullanım yöntemlere göre kıyaslarsak, bu tezde kullanılan algoritmanın daha basit olduğu belirtilebilir.

1. INTRODUCTION

Tracking the maximum power point (MPP) of a photovoltaic (PV) array is usually an essential part of a PV system. As such, many MPP tracking (MPPT) methods have been developed and implemented. The methods vary in complexity, sensors required, convergence speed, cost, range of effectiveness, implementation hardware, popularity, and in other respects. They range from the almost obvious (but not necessarily ineffective) to the most creative (not necessarily most effective). In fact, so many methods have been developed that it has become difficult to adequately determine which method, newly proposed or existing, is most appropriate for a given PV system.

1.1 Problem Overview

Figure 1.1 shows the characteristic power curve for a PV array. The problem considered by MPPT techniques is to automatically find the voltage V_{MPP} or current I_{MPP} at which a PV array should operate to obtain the maximum power output P_{MPP} under a given temperature and irradiance. It is noted that under partial shading conditions, in some cases it is possible to have multiple local maxima, but overall there is still only one true MPP. Most techniques respond to changes in both irradiance and temperature, but some are specifically more useful if temperature is approximately constant. Most techniques would automatically respond to changes in the array due to aging, though some are open-loop and would require periodic fine-tuning. In our context, the array will typically be connected to a power converter that can vary the current coming from the PV array [3].

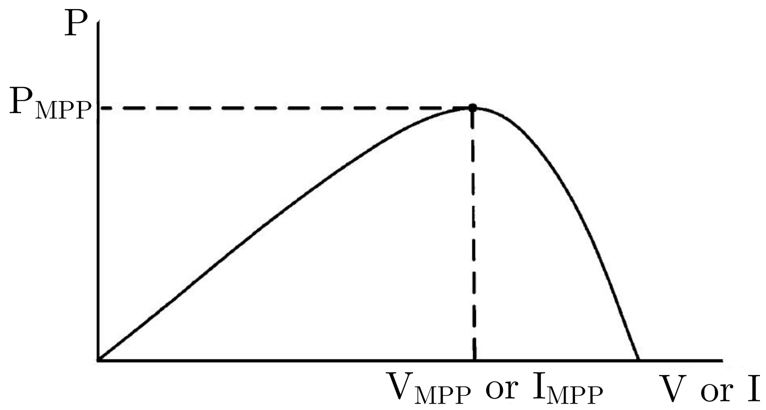

Figure 1.1: Characteristic PV array power curve.

1.2 Maximum Power Point Technique

The different MPPT techniques are discussed below in an arbitrary order.

1.2.1 Hill Climbing/Perturb and Observe

Among the papers, much focus has been on hill climbing, and perturb and observe (P&O) methods. Hill climbing involves a perturbation in the duty ratio of the power converter, and P&O a perturbation in the operating voltage of the PV array. In the case of a PV array connected to a power converter, perturbing the duty ratio of power converter perturbs the PV array current and consequently perturbs the PV array voltage. Hill climbing and P&O methods are different ways to envision the same fundamental method. From Figure 1.1, it can be seen that incrementing (decrementing) the voltage increases (decreases) the power when operating on the left of the MPP and decreases (increases) the power when on the right of the MPP. Therefore, if there is an increase in power, the subsequent perturbation should be kept the same to reach the MPP and if there is a decrease in power, the perturbation should be reversed. The algorithm also works when instantaneous (instead of average) PV array voltage and current are used, as long as sampling occurs only once in each switching cycle. The process is repeated periodically until the MPP is reached. The system then oscillates about the MPP. The oscillation can be minimized by reducing the perturbation step size. However, a smaller perturbation size slows down the MPPT. A solution to this conflicting situation is to have a variable perturbation size that gets smaller towards the MPP. Fuzzy logic control is used to optimize the magnitude of the next perturbation. In a method, a two-stage algorithm is proposed that offers faster tracking in the first stage and finer tracking in the second stage. On the other hand, another method by passes the first stage by using a nonlinear equation to estimate an initial operating point close to the MPP.

Hill climbing and P&O methods can fail under rapidly changing atmospheric conditions as illustrated in Figure 1.2. Starting from an operating point A, if atmospheric conditions stay approximately constant, a perturbation ΔVin the PV voltage V will bring the operating point to B and the perturbation will be reversed due to a decrease in power. However, if the irradiance increases and shifts the power curve from P1 to P2 within one sampling period, the operating point will move from A to C. This represents an increase in power and the perturbation is kept the same. Consequently, the operating point diverges from the MPP and will keep diverging if the irradiance steadily increases. To ensure that the MPP is tracked even under sudden changes in irradiance, uses a three-point weight comparison P&O method that compares the actual power point to two preceding ones before a decision is made about the perturbation sign. Two sensors are usually required to measure the PV array voltage and current from which power is computed, but depending on the power converter topology, only a voltage sensor might be needed. In some methods, the PV array current from the PV array voltage is estimated, eliminating the need for a current sensor. DSP or microcomputer control is more suitable for hill climbing and P&O even though discrete analog and digital circuitry can be used. P&O is more suitable for PV grid-connected converter system. Hill climbing MPPT strategy is more suitable for battery charger with which the fast dynamic response requirement is not necessary [4].

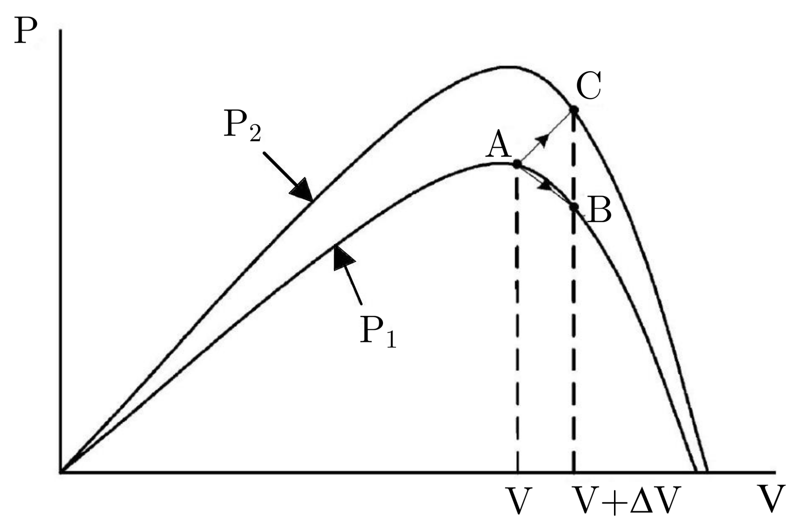

Figure 1.2: Divergence of hill climbing/P&O from MPP.

1.2.2 Incremental Conductance

The incremental conductance (IncCond), method is based on the fact that the slope of the PV array power curve (Figure 1.2) is zero at the MPP, positive on the left of the MPP, and negative on the right, as given by

$$\begin{cases} dP/dV = 0; & \text{at MPP.} \\ dP/dV > 0; & \text{left of MPP.} \\ dP/dV < 0; & \text{right of MPP.} \end{cases} \tag{1.1}$$

since

$$\frac{dP}{dV} = \frac{d\,(IV)}{dV} = I + V\frac{dI}{dV} \cong I + V\frac{\Delta I}{\Delta V} \tag{1.2}$$

Equation 1.1 can be rewritten as

$$\begin{cases} \Delta I/\Delta V = -I/V; & \text{at MPP.} \\ \Delta I/\Delta V > -I/V; & \text{left of MPP.} \\ \Delta I/\Delta V < -I/V; & \text{right of MPP.} \end{cases} \tag{1.3}$$

The MPP can thus be tracked by comparing the instantaneous conductance (I/V) to the incremental conductance$(\Delta I/\Delta V)$ as shown in the flowchart in Figure 1.3. V_{ref} is the reference voltage at which the PV array is forced to operate. At the MPP, V_{ref} equals to V_{MPP}. Once the MPP is reached, the operation of the PV array is maintained at this point unless a change in ΔI is noted, indicating a change in atmospheric conditions and the MPP. The algorithm decrements or increments V_{ref} to track the new

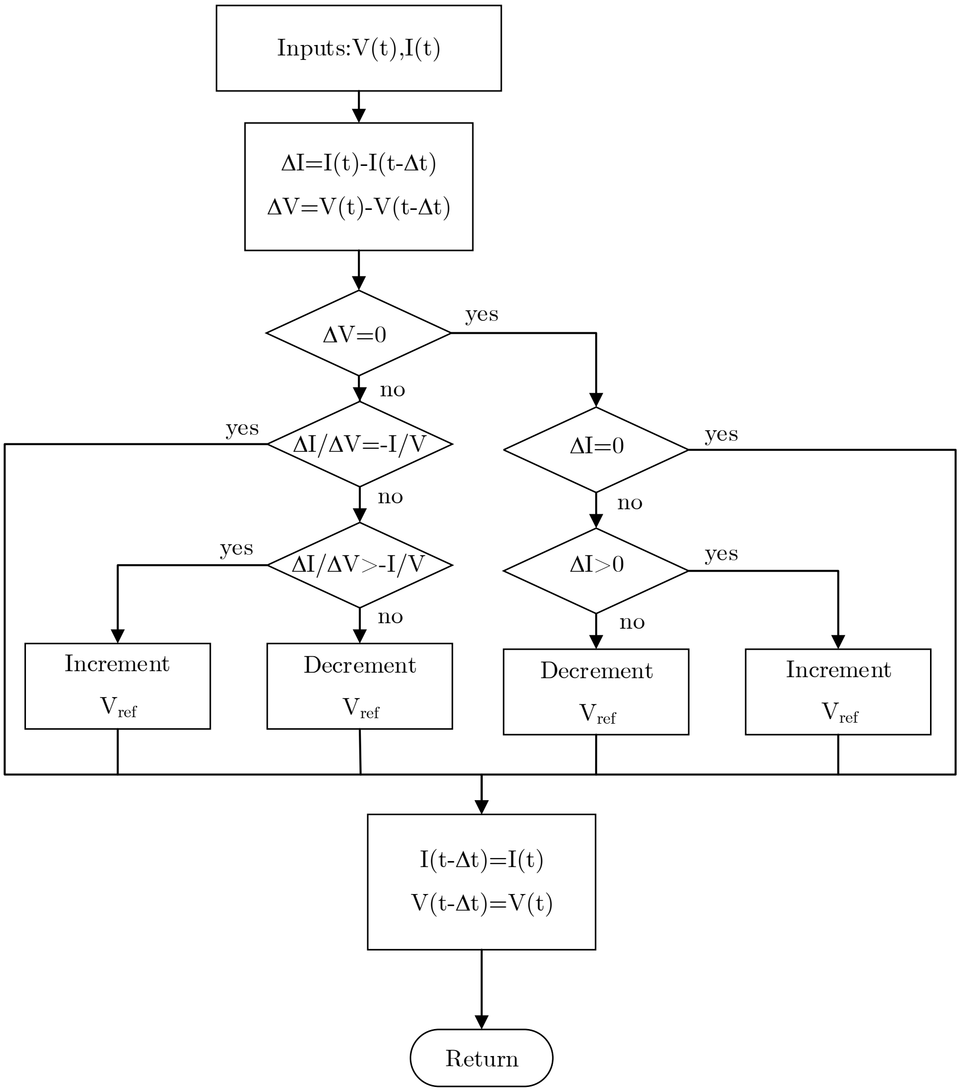

Figure 1.3: Incremental Conductance algorithm.

MPP [5]. The increment size determines how fast the MPP is tracked. Fast tracking can be achieved with bigger increments but the system might not operate exactly at the MPP and oscillate about it instead; so there is a tradeoff. In a some methods, method is proposed that brings the operating point of the PV array close to the MPP in a first stage and then uses IncCond to exactly track the MPP in a second stage. By proper control of the power converter, the initial operating point is set to match a load resistance proportional to the ratio of the open-circuit voltage (V_{OC}) to the short-circuit current (I_{SC}) of the PV array. This two stage alternative also ensures that the real MPP is tracked in case of multiple local maxima.

In another method a linear function is used to divide the I–V plane into two areas, one containing all the possible MPPs under changing atmospheric conditions. The operating point is brought into this area and then IncCond is used to reach the MPP.

A less obvious, but effective way of performing the IncCond technique is to use the instantaneous conductance and the incremental conductance to generate an error signal

$$e = \frac{I}{V} + \frac{dI}{dV} \tag{1.4}$$

From Equation 1.1, we know that e goes to zero at the MPP. A simple proportional integral (PI) control can then be used to drive e to zero. Measurements of the instantaneous PV array voltage and current require two sensors. IncCond method lends itself well to DSP and microcontroller control, which can easily keep track of previous values of voltage and current and make all the decisions as per Figure 1.3 [6].

1.2.3 Fractional Open-Circuit Voltage

The near linear relationship between V_{MPP} and V_{OC} of the PV array, under varying irradiance and temperature levels, has given rise to the fractional V_{OC} method

$$V_{MPP} \approx k_1 V_{OC} \tag{1.5}$$

where k_1 is a constant of proportionality. Since k_1 is dependent on the characteristics of the PV array being used, it usually has to be computed beforehand by empirically determining V_{MPP} and V_{OC} for the specific PV array at different irradiance and temperature levels. The factor k_1 has been reported to be between 0.71 and 0.78. Once k_1 is known, V_{MPP} can be computed using Equation 1.5 with V_{OC} measured periodically by momentarily shutting down the power converter. However, this incurs some disadvantages, including temporary loss of power. To prevent this, a method uses pilot cells from which V_{OC} can be obtained. These pilot cells must be carefully chosen to closely represent the characteristics of the PV array [3]. the voltage generated by pn-junction diodes is approximately 75% of V_{OC} [7]. This eliminates the need for measuring V_{OC} and computing V_{MPP}. Once V_{MPP} has been approximated, a closed-loop control on the array power converter can be used to asymptotically reach this desired voltage.

Since Equation 1.5 is only an approximation, the PV array technically never operates at the MPP. Depending on the application of the PV system, this can sometimes be adequate. Even if fractional V_{OC} is not a true MPPT technique, it is very easy and cheap to implement as it does not necessarily require DSP or microcontroller control. However, k_1 is no more valid in the presence of partial shading (which causes multiple local maxima) of the PV array and proposes sweeping the PV array voltage to update k_1. This obviously adds to the implementation complexity and incurs more power loss [8].

1.2.4 Fractional Short-Circuit Current

Fractional I_{SC} results from the fact that, under varying atmospheric conditions, I_{MPP} is approximately linearly related to the I_{SC} of the PV array

$$I_{MPP} \approx k_2 I_{SC} \quad \textbf{(1.6)}$$

where k_2 is a proportionality constant. Just like in the fractional V_{OC} technique, k_2 has to be determined according to the PV array in use. The constant k_2 is generally found to be between 0.78 and 0.92.

Measuring I_{SC} during operation is problematic. An additional switch usually has to be added to the power converter to periodically short the PV array so that I_{SC} can be measured using a current sensor. This increases the number of components and cost. Power output is not only reduced when finding I_{SC} but also because the MPP is never perfectly matched. One way of compensating k_2 is proposed such that the MPP is better tracked while atmospheric conditions change. To guarantee proper MPPT in the presence of multiple local maxima, in some method periodically sweeps the PV array voltage from open-circuit to short-circuit to update k_2. Most of the PV systems using fractional I_{SC} in the literature use a DSP. In a method, a simple current feedback control loop is used instead [9].

1.2.5 Fuzzy Logic Control

Microcontrollers have made using fuzzy logic control popular for MPPT over the last decade. Fuzzy logic controllers have the advantages of working with imprecise inputs, not needing an accurate mathematical model, and handling nonlinearity. Fuzzy logic control generally consists of three stages: fuzzification, rule base table lookup, and defuzzification. During fuzzification, numerical input variables are converted into linguistic variables based on a membership function .

The inputs to a MPPT fuzzy logic controller are usually an error E and a change in error ΔE. The user has the flexibility of choosing how to compute E and ΔE. Since dP/dV vanishes at the MPP, by use the approximation

$$E(n) = \frac{P(n) - P(n-1)}{V(n) - V(n-1)} \quad \textbf{(1.7)}$$

and

$$\Delta E(n) = E(n) - E(n-1) \quad \textbf{(1.8)}$$

Equivalently, Equation 1.4 is very often used. Once E and ΔE are calculated and converted to the linguistic variables, the fuzzy logic controller output, which is typically a change in duty ratio ΔD of the power converter, can be looked up in a rule base table.

The linguistic variables assigned to ΔD for the different combinations of E and ΔE are based on the power converter being used and also on the knowledge of the user.

In the defuzzification stage, the fuzzy logic controller output is converted from a linguistic variable to a numerical variable still using a membership function. This provides an analog signal that will control the power converter to the MPP. MPPT fuzzy logic controllers have been shown to perform well under varying atmospheric conditions. However, their effectiveness depends a lot on the knowledge of the user or control engineer in choosing the right error computation and coming up with the rule base table [10].

1.2.6 Neural Network

Along with fuzzy logic controllers came another technique of implementing MPPT—neural networks, which are also well adapted for microcontrollers. Neural networks commonly have three layers: input, hidden, and output layers as shown in Figure 1.4. The number of nodes in each layer vary and are user-dependent. The input variables can be PV array parameters like V_{OC} and I_{SC}, atmospheric data like irradiance and temperature, or any combination of these. The output is usually one or several reference signal(s) like a duty cycle signal used to drive the power converter to operate at or close to the MPP.

How close the operating point gets to the MPP depends on the algorithms used by the hidden layer and how well the neural network has been trained. The links between the nodes are all weighted. The link between nodes i and j is labeled as having a weight of w_{ij} in Figure 1.4. To accurately identify the MPP, the w_{ij} have to be carefully

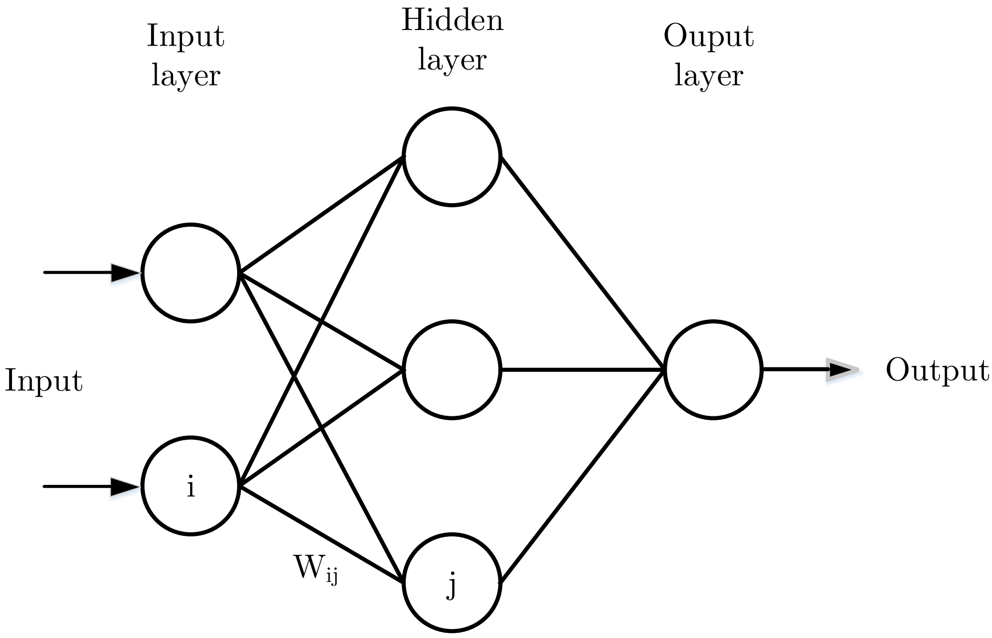

Figure 1.4: Example of neural network.

determined through a training process, whereby the PV array is tested over months or years and the patterns between the input(s) and output(s) of the neural network are recorded.

Since most PV arrays have different characteristics, a neural network has to be specifically trained for the PV array with which it will be used. The characteristics of a PV array also change with time, implying that the neural network has to be periodically trained to guarantee accurate MPPT [11].

1.2.7 Ripple Correlation Control

When a PV array is connected to a power converter, the switching action of the power converter imposes voltage and current ripple on the PV array. As a consequence, the PV array power is also subject to ripple. Ripple correlation control (RCC) makes use of ripple to perform MPPT. RCC correlates the time derivative of the time-varying PV array power $\dot{p}$ with the time derivative of the time-varying PV array current $\dot{i}$ or voltage $\dot{v}$ to drive the power gradient to zero, thus reaching the MPP.

Referring to Figure 1.1, if v or i is increasing ($\dot{v}$> 0 or $\dot{i}$ > 0) and p is increasing ($\dot{v}$ > 0), then the operating point is below the MPP (V <V_{MPP} or I < I_{MPP}). On the other hand, if v or i is increasing and p is decreasing ($\dot{p}$ < 0), then the operating point is above the MPP (V >V_{MPP} or I > I_{MPP}). Combining these observations, we see that $\dot{p}\dot{v}$ or $\dot{p}\dot{i}$ are positive to the left of the MPP, negative to right of the MPP, and zero at the MPP. When the power converter is a boost converter increasing the duty ratio increases the inductor current, which is the same as the PV array current, but decreases the PV array voltage. Therefore, the duty ratio control input is

$$d(t) = -k_3 \int \dot{p}\dot{v}\, dt \tag{1.9}$$

or

$$d(t) = -k_3 \int \dot{p}\dot{i}\, dt \tag{1.10}$$

where k_3 is a positive constant. Controlling the duty ratio in this fashion assures that the MPP will be continuously tracked, making RCC a true MPP tracker.

The derivatives in Equation 1.9 and Equation 1.10 are usually undesirable, but ac-coupled measurements of the PV array current and voltage can be used instead since they contain the necessary phase information.

The derivatives can also be approximated by high-pass filters with cut-off frequency higher than the ripple frequency. A different and easy way of obtaining the current derivative in Equation 1.10 is to sense the inductor voltage, which is proportional to the current derivative. The nonidealities in the inductor (core loss, resistance) have a small effect since the time constant of the inductor is much larger than the switching period in a practical converter.

Equation 1.10 can fail due to the phase shift brought about by the intrinsic capacitance of the PV array at high switching frequency. However, correlating power and voltage as in Equation 1.9 is barely affected by the intrinsic capacitance.

Simple and inexpensive analog circuits can be used to implement RCC. Experiments were performed to show that RCC accurately and quickly tracks the MPP, even under varying irradiance levels. The time taken to converge to the MPP is limited by the switching frequency of the power converter and the gain of the RCC circuit. Another advantage of RCC is that it does not require any prior information about the PV array characteristics, making its adaptation to different PV systems straightforward [12].

1.2.8 Current Sweep

The current sweep method uses a sweep waveform for the PV array current such that the I–V characteristic of the PV array is obtained and updated at fixed time intervals. The V_{MPP} can then be computed from the characteristic curve at the same intervals.

The function chosen for the sweep waveform is directly proportional to its derivative as in

$$f(t) = k_4 \frac{df(t)}{dt} \tag{1.11}$$

where k_4 is a proportionality constant. The PV array power is thus given by

$$p(t) = v(t)i(t) = v(t)f(t). \tag{1.12}$$

at the MPP

$$\frac{dp(t)}{dt} = v(t)\frac{df(t)}{dt} + f(t)\frac{dv(t)}{dt} = 0. \tag{1.13}$$

Substituting Equation 1.11 in Equation 1.13 gives

$$\frac{dp(t)}{dt} = \left[v(t) + k_4 \frac{dv(t)}{dt}\right] \frac{df(t)}{dt} = 0. \tag{1.14}$$

The differential equation in 1.11 has the following solution

$$f(t) = C\, e^{[t/k_4]} \tag{1.15}$$

C is chosen to be equal to the maximum PV array current I_{max} and k_4 to be negative, resulting in a decreasing exponential function with time constant $\tau = k_4$. Equation 1.15 leads to

$$f(t) = I_{max}\, e^{[-t/\tau]}. \tag{1.16}$$

The current in Equation 1.16 can be easily obtained by using some current discharging through a capacitor. Since the derivative of Equation 1.16 is nonzero, Equation 1.14 can be divided throughout by df $(t)/dt$ and, with $f(t) = i(t)$, Equation1.14simplifies to

$$\frac{dp(t)}{di(t)} = v(t) + k_4 \frac{dv(t)}{dt} = 0 \tag{1.17}$$

Once V_{MPP} is computed after the current sweep, Equation 1.17 can be used to double check whether the MPP has been reached. The current sweep method is implemented through analog computation. The current sweep takes about 50 ms, implying some loss of available power. This MPPT technique is only feasible if the power consumption of the tracking unit is lower than the increase in power that it can bring to the entire PV system [13].

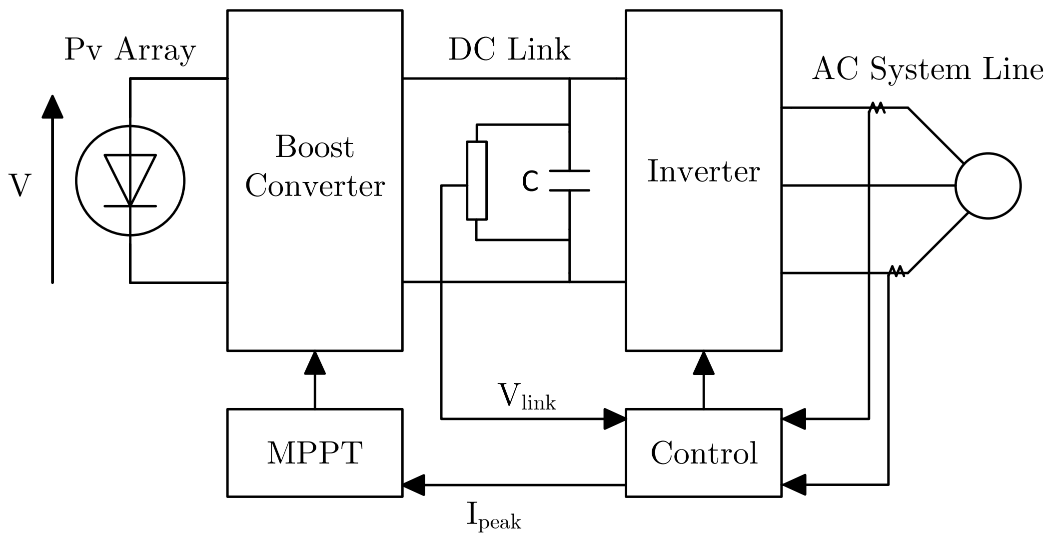

Figure 1.5: Topology for dc-link capacitor droop control.

1.2.9 DC-Link Capacitor Droop Control

DC-link capacitor droop control is an MPPT technique that is specifically designed to work with a PV system that is connected in parallel with an ac system line as shown in Figure 1.5.

The duty ratio of an ideal boost converter is given by

$$d = 1 - \frac{V}{V_{Link}} \tag{1.18}$$

where V is the voltage across the PV array and V_{link} is the voltage across the dc link. If V_{link} is kept constant, increasing the current going in the inverter increases the power coming out of the boost converter and consequently increases the power coming out of the PV array. While the current is increasing, the voltage V_{link} can be kept constant as long as the power required by the inverter does not exceed the maximum power available from the PV array. If that is not the case, V_{link} starts drooping. Right before that point, the current control command I_{peak} of the inverter is at its maximum and the PV array operates at the MPP. The ac system line current is fed back to prevent V_{link} from drooping and d is optimized to bring I_{peak} to its maximum, thus achieving MPPT. DC-link capacitor droop control does not require the computation of the PV array power, but, its response deteriorates when compared to a method that detects the power directly; this is because its response directly depends on the response of the dc-voltage control loop of the inverter. This control scheme can be easily implemented with analog operational amplifiers and decision-making logic units [14].

1.2.10 Load Current or Load Voltage Maximization

The purpose of MPPT techniques is to maximize the power coming out of a PV array. When the PV array is connected to a power converter, maximizing the PV array power also maximizes the output power at the load of the converter. Conversely, maximizing the output power of the converter should maximize the PV array power, assuming a lossless converter.

It is pointed out that most loads can be of voltage-source type, current-source type, resistive type, or a combination of these, it is clear that for a voltage-source type load, the load current i_{out} should be maximized to reach the maximum output power. For a current-source type load, the load voltage v_{out} should be maximized.

For the other load types, either i_{out} or v_{out} can be used. This is also true for nonlinear load types as long as they do not exhibit negative impedance characteristics. Therefore, for almost all loads of interest, it is adequate to maximize either the load current or the load voltage to maximize the load power. Consequently, only one sensor is needed. In most PV systems, a battery is used as the main load or as a backup. Since a battery can be thought of as a voltage-source type load, the load current can be used as the control variable. In this methods positive feedback is used to control the power converter such that the load current is maximized and the PV array operates close to the MPP. Operation exactly at the MPP is almost never achieved because this MPPT method is based on the assumption that the power converter is lossless [15].

1.2.11 *d*P/*d*V or *d*P/*d*I Feedback Control

With DSP and microcontroller being able to handle complex computations, an obvious way of performing MPPT is to compute the slope $(dP/dV\, or dP/dI)$ of the PV power curve (Figure 1.1) and feed it back to the power converter with some control to drive it to zero.

The way the slope is computed differs from paper to paper. In a method, dP/dV is computed and its sign is stored for the past fewcycles. Based on these signs, the duty ratio of the power converter is either incremented or decremented to reach the

MPP. A dynamic step size is used to improve the transient response of the system [16]. In [17] the PV array voltage is periodically incremented or decremented and $\Delta P/\Delta V$ is compared to a marginal error until the MPP is reached.

1.2.12 Other MPPT Techniques

Other MPPT techniques include array reconfiguration, whereby PV arrays are arranged in different series and parallel combinations such that the resulting MPPs meet specific load requirements. This method is time consuming and tracking MPP in real time is not obvious [18].

In a different method linear current control is used based on the fact that a linear relationship exists between I_{MPP} and the level of irradiance. The current I_{MPP} is thus found by sensing the irradiance level and a PI controller is used such that the PV array current follows I_{MPP} [19].

In another technique, I_{MPP} and V_{MPP} are computed from equations involving temperature and irradiance levels, which are not usually easy to measure. Once I_{MPP} or V_{MPP} is obtained, feedback control is used to force the PV array to operate at the MPP [20].

In state-based MPPT method system is represented by a state space model, and a nonlinear time varying dynamic feedback controller is used to track the MPP [21]. Simulations confirm that this technique is robust and insensitive to changes in system parameters and that MPPT is achieved even with changing atmospheric conditions and in the presence of multiple local maxima caused by partially shaded PV array or damaged cells.

Unlike common topologies that consist of two power stages (usually a dc–dc converter followed by an inverter), a single stage is inverter that performs both MPPT and output current regulation for utility grid distribution. Based on the voltage of the PV array, one-cycle control (OCC) is used to adjust the output current of the single-stage inverter such that MPPT is attained. The control circuit consists of discrete digital components but it can also use an inexpensive DSP. Operation is shown to be close to the MPP throughout a daytime period. The slight discrepancy is due to the inability of the controller to account for temperature variation.

In best fixed voltage (BFV) algorithm statistical data is collected about irradiance and temperature levels over a period of one year and the BFV representative of the MPP is found. The control sets either the operating point of the PV array to the BFV or the output voltage to the nominal load voltage. Operation is therefore never exactly at the MPP and different data has to be collected for different geographical regions [22].

The PV array characteristic equation, which needs to be solved iteratively for the MPP, is manipulated to find an approximate symbolic solution for the MPP in another method. This method, called linear reoriented coordinates method (LRCM), requires the measurement of V_{OC} and I_{SC} to find the solution. Other constants representing the PV array characteristic curve are also needed. The maximum error in using LRCM to approximate the MPP was found to be 0.3 ٪ , but this was based only on simulation results [23].

Slide control method with a buck-boost converter is used to achieve MPPT [24]. The switching function u of the converter is based on the fact that $dP/dV > 0$ on the left of the MPP and $dP/dV < 0$ on the right; u is expressed as

$$\begin{cases} u = 0; & S \geq 0 \\ u = 1; & S < 0 \end{cases} \quad \textbf{(1.19)}$$

where $u = 0$ means the switch is open and $u = 1$ the switch close and S is given by

$$S = \frac{dP}{dV} = I + V\frac{dI}{dV} \quad \textbf{(1.20)}$$

This control was implemented using a microcontroller that senses the PV array voltage and current.

1.3 Discussion

With so many MPPT techniques available to PVsystem users, it might not be obvious for the latter to choose which one better suits their application needs. The main aspects of the MPPT techniques to be taken into consideration are highlighted in the following subsections.

1.3.1 Implementation

The ease of implementation is an important factor in deciding which MPPT technique to use. However, this greatly depends on the end-users'knowledge. Some might be more familiar with analog circuitry, in which case, fractional I_{SC} or V_{OC}, RCC, and load current or voltage maximization are good options. Others might be willing to work with digital circuitry, even if that may require the use of software and programming. Then, their selection should include hill climbing/P&O, IncCond, fuzzy logic control, neural network, and dP/dV or dP/dI feedback control. Furthermore, a few of the MPPT techniques only apply to specific topologies. For example, the dc-link capacitor droop control works with the system shown in Figure 1.5 and the OCC MPPT works with a single-stage inverter.

1.3.2 Sensors

The number of sensors required to implement MPPT also affects the decision process. Most of the time, it is easier and more reliable to measure voltage than current. Moreover, current sensors are usually expensive and bulky. This might be inconvenient in systems that consist of several PV arrays with separate MPP trackers. In such cases, it might be wise to use MPPT methods that require only one sensor or that can estimate the current from the voltage. It is also uncommon to find sensors that measure irradiance levels, as needed in the linear current control and the I_{MPP} and V_{MPP} computation methods.

1.3.3 Multiple Local Maxima

The occurrence of multiple local maxima due to partial shading of the PV array(s) can be a real hindrance to the proper functioning of an MPP tracker. Considerable power loss can be incurred if a local maximum is tracked instead of the real MPP. As mentioned previously, the current sweep and the state based methods should track the true MPP even in the presence of multiple local maxima. However, the other methods require an additional initial stage to bypass the unwanted local maxima and bring operation to close the real MPP.

1.3.4 Cost

It is hard to mention the monetary costs of every single MPPT technique unless it is built and implemented. However, a good costs comparison can be made by knowing whether the technique is analog or digital, whether it requires software and programming, and the number of sensors. Analog implementation is generally cheaper than digital, which normally involves a microcontroller that needs to be programmed. Eliminating current sensors considerably drops the costs.

1.3.5 Application

Different MPPT techniques discussed earlier will suit different applications. For example, in space satellites and orbital stations that involve large amount of money, the costs and complexity of the MPP tracker are not as important as its performance and reliability. The tracker should be able to continuously track the true MPP in minimum amount of time and should not require periodic tuning. In this case, hill climbing/P&O, IncCond, and RCC are appropriate. Solar vehicles would mostly require fast convergence to the MPP. Fuzzy logic control, neural network, and RCC are good options in this case. Since the load in solar vehicles consists mainly of batteries, load current or voltage maximization should also be considered. The goal when using PV arrays in residential areas is to minimize the payback time and to do so, it is essential to constantly and quickly track the MPP. Since partial shading (from trees and other buildings) can be an issue, the MPPT should be capable of bypassing multiple local maxima. Therefore, the two-stage IncCond and the current sweep methods are suitable. Since a residential system might also include an inverter, the OCC MPPT can also be used. PV systems used for street lighting only consist in charging up batteries during the day. They do not necessarily need tight constraints; easy and cheap implementation might be more important, making fractional V_{OC} or I_{SC} viable. For all other applications not mentioned here, Table 1.1, containing the major characteristics of all the MPPT techniques. Table 1.1 should help in choosing an appropriate MPPT method.

Table 1.1: Comparison of various MPPT algorithms.

MPPT Technique	PV Array Dependent?	True MPPT?	Analog or Digital?	Periodic Tuning?	Convergence Speed	Implementation Complexity	Sensed Parameters
Hill Climbing/P&O	No	Yes	Both	No	Varies	Low	Voltage,Current
Incremental Conductance	No	Yes	Digital	No	Varies	Medium	Voltage,Current
Fractional V_{oc}	Yes	No	Both	Yes	Medium	Low	Voltage
Fractional I_{sc}	Yes	No	Both	Yes	Medium	Medium	Current
Fuzzy Logic Control	Yes	Yes	Digital	Yes	Fast	High	Varies
Neural Network	Yes	Yes	Digital	Yes	Fast	High	Varies
RCC	No	Yes	Analog	No	Fast	Low	Voltage,Current
Current Sweep	Yes	Yes	Digital	Yes	Slow	High	Voltage,Current
DC-Link Capacitor Droop Control	No	No	Both	No	Medium	Low	Voltage
Load I or V Maximization	No	No	Analog	No	Fast	Low	Voltage,Current
dP/dV or dP/dI Feedback Control	No	Yes	Digital	No	Fast	Medium	Voltage,Current
Array Reconfiguration	Yes	No	Digital	Yes	Slow	High	Voltage,Current
Linear Current Control	Yes	No	Digital	Yes	Fast	Medium	Irradiance
I_{MPP} & V_{MPP} computation	No	Yes	Digital	Yes	N/A	Medium	Irradiance,temperature
State-based MPPT	Yes	Yes	Both	Yes	Fast	High	Voltage,Current
OCC MPPT	Yes	No	Both	Yes	Fast	Medium	Current
BFV	Yes	No	Both	Yes	N/a	Low	None
LRCM	Yes	No	Digital	No	N/A	High	Voltage,Current
Slide Control	No	Yes	Digital	No	Fast	Medium	Voltage,Current

1.4 Contribution of Thesis

This thesis proposes a reliable MPPT scheme based on PSO algorithm. The PSO algorithm tracks the optimal power point by searching the PV array voltage at maximum power point (VMPP). Once the VMPP is identified, the actual PV array voltage is controlled to such optimal value computed by the PSO algorithm. The PV module is forced to operate at such optimal operating point with the aid of a power conditioner (dc boost) driven by On/Off voltage controller with microcontroller.

In this algorithm which is base on PO method we just need a current sensor and microcontroller (In this thesis AVR ATmega32 is used) and boost converter. One of the important specification of PSO algorithm is tracking global maximum point even in presence of multiple local maximums.

Versus of other method which use microcontroller like look table-up method, this method does not need any information about panel and environment condition i.e, we can use this controller for any panel in any condition also changing of temperature and irradiation does not affect operation.

This method does not need any control loop so it is low cost, which does process with AVR microcontroller and current sensor. By comparing this algorithm with other intelligent systems like fuzzy controller or neural network system this algorithm is more simple.

2. MODELING OF PHOTOVOLTAIC CELL

2.1 Introduction

There are numerous studies that develop the mathematical modeling of photovoltaic cells and verified by software, like the methods in [25], [26]. The model presented is based on an equivalent circuit implemented in software. Software uses a generic diode for adjust the current and voltage curve (IV curve) at photovoltaic cell.
The model of PV cell can be used to simulate a PV module, because PV module is an association of cells in series and parallel. The model PV module can use to study mismatch effects due to different electrical characteristics of PV cells and the use of pass diode to reduce loss due to partial shadows.

2.2 Equivalent circuit of photovoltaic cell

The equivalent circuit of an ideal cell is formed by a current source in parallel with a diode. There are several circuits that include resistors for real effects of a photovoltaic cell, the circuit of Figure 2.1 is the more commonly used. Although several simulations simplifies the parallel resistance value with a high value, using the series resistance to include effect of fill factor, gets a similar circuit and used R_p to avoid problem with simulation. Then this circuit has a simple and accurate model to simulate a photovoltaic cell.
The problem is the parameter values of circuit components, in this Section parameters are calculated by using data from the photovoltaic cell indicated in datasheets, for equivalent circuit on Figure 2.1 .

2.3 Current-Voltage (IV) Curve

For calculate equivalent circuit parameters, it is essential to obtain the IV curve. In the IV curve Figure 2.2, it can extract the electrical characteristics of the photovoltaic cell in standard test conditions (STC).

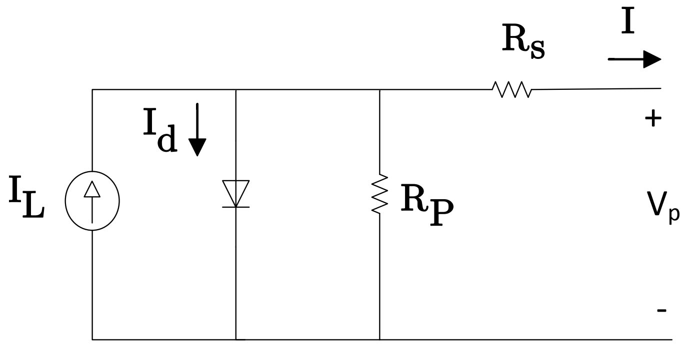

Figure 2.1: Equivalent circuit of photovoltaic cell.

I_{SC} (short circuit current) is maximum intensity that can generate a photovoltaic cell or module when measuring the current if performing a short circuit (output voltage of 0 volts). V_{OC} (open circuit voltage) is maximum voltage that can generate a photovoltaic cell or module when measuring the voltage if not flowing current (current of 0 amps). P_{MAX} (Maximum power) is maximum power that can generate a photovoltaic cell or module and it is the product of maximum voltage and current. V_{MAX} (Maximum Voltage) is the voltage at maximum power (around 80⁒ of open circuit voltage) and I_{MAX} (Maximum Current) is the current at maximum power. By consider equivalent circuit Figure 2.1, value of I_{SC} related with I_L and value of V_{OC} related with diode current (I_d), then diode includes effects of exponential of IV curve. Finally R_s adjusts value of P_{MAX}. All parameter information is extract to datasheets, and STC are: 25ºC for cell temperature (T_C), 1000 W/m^2 for irradiance (G) and 3m/s for wind speed.

2.4 Modeling equations of photovoltaic cell

Reference to the circuit of Figure 2.1, then show all equations needed to obtain all the parameters that define the model in STC. In Equation 2.1 shows the intensity value generated by the photovoltaic cell [27]. I is output current of photovoltaic cell, V is output voltage of photovoltaic cell, I_L is the photogenerated current, I_0 is the saturation current of diode, R_S is series resistance due to the junction between the semiconductor and the metal contacts (interconnects), R_P is parallel resistance due to no linearity of union PN, m is ideal factor of diode and V_t is thermal voltage shown in Equation 2.2 (where: k is Boltzmann constant and equal to 1.3807×10^{-23} joule per kelvin, q is electron charge equal to 1.602×10^{19} coulomb

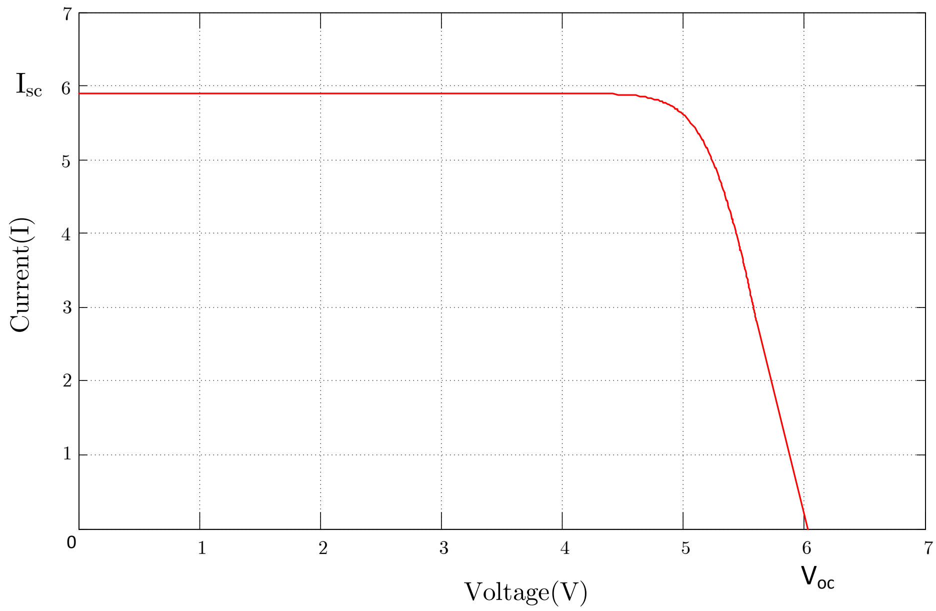

Figure 2.2: IV Curve of photovoltaic module.

and T is temperature in degree Kelvin).

$$I = I_L - I_0 \left[e^{\left(\frac{V + I \cdot R_s}{m \cdot V_t} \right)} - 1 \right] - \left[\frac{V + I \cdot R_s}{R_p} \right] \quad \textbf{(2.1)}$$

$$V_t = \frac{k \cdot T}{q} \quad \textbf{(2.2)}$$

Equation 2.1 can simplify the last term with a high value of R_P (for example 100k Ω). Furthermore, I_L is considered equal to the short circuit current in STC (I_{SC_STC}) [25]. Then we obtain the Equation 2.3 at STC.

$$I = I_{SC\_STC} - I_{0\_STC} \left[e^{\left(\frac{V + I \cdot R_s}{m \cdot V_t} \right)} - 1 \right] \quad \textbf{(2.3)}$$

The value of I_0 is obtained for STC (I_{0_STC}) using Equation 2.4, based on [26], considering open voltage circuit in STC (V_{OC_STC}) and cell temperature in STC (T_{C_STC}).

$$I_{0\_STC} = \frac{I_{SC\_STC}}{\left(e^{\left(\frac{q \cdot V_{OC\_STC}}{m \cdot k \cdot T_{C\_STC}}\right)} - 1\right)} \tag{2.4}$$

There is an empirical relationship between the value of V_{OC_STC} and I_{SC_STC} with R_S [27]. Then, needs calculate fill factor of ideal device (FF_0) at Equation 2.5, using parameter v_{oc} of Equation 2.6, and calculate R_S using Equation 2.8. The fill factor (FF) of photovoltaic cell shows at Equation 2.7. This approach only use when R_P value is high, therefore fill factor depends of R_S value.

$$FF_0 = \frac{v_{oc} - \ln(v_{oc} + 0.72)}{v_{oc} + 1} \tag{2.5}$$

$$v_{oc} = \frac{V_{OC\_STC}}{V_t} \tag{2.6}$$

$$FF = \frac{V_{MAX\_STC} \cdot I_{MAX\_STC}}{I_{SC\_STC} \cdot V_{OC\_STC}} \tag{2.7}$$

$$R_s = \left(1 - \frac{FF}{FF_0}\right) \cdot \left(\frac{V_{OC\_STC}}{I_{SC\_STC}}\right) \tag{2.8}$$

Changes in temperature affect the values of I_{SC}, V_{oc} and P_{MAX}, when cell temperature increase the V_{OC} decrease, same with the P_{MAX}, α and β establishing the relationship between units (voltage, current and power) and temperature.
Also when irradiation increase the I_{SC} also increase. Also changes in irradiance (G), affect the value of I_{SC} and V_{OC}. Therefore, using approximation of Luque-Sala and Duffie&Beckman, we obtain the Equation 2.9 for I_L [28]. Besides empirical tests simulation to study the effects of temperature on I_0, used for get Equation 2.10, based on the approximation Duffie&Beckman.

$$I_L = I_{SC\_STC} \cdot \frac{G}{G_{STC}} \cdot (1 + \alpha \cdot (T_C - T_{C\_STC})) \tag{2.9}$$

$$I_0 = \frac{I_{SC\_STC} \cdot \frac{G}{G_{STC}} \cdot (1 + \alpha \cdot (T_C - T_{C\_STC}))}{\left(e^{\left(q \cdot \frac{(V_{OC\_STC} + \beta \cdot (T_C - T_{SC\_STC}))}{m \cdot k \cdot T_{C\_STC}}\right)} - 1\right)} \tag{2.10}$$

The relationship between temperature ambient (T_A) and cell (T_C), can used Equations 2.11 and 2.12, [29]. It is based on normal operating temperature cell (T_{NOC}), is defined as the average temperature of equilibrium within a photovoltaic cell to an irradiance of $800W/m^2$ and an outside temperature of 20ºC. Use of this approximation is interesting because there are statistics of temperature ambient on geographic situation but temperature cell depends to PV cell and module.

$$T_C - T_A = C \cdot G \Rightarrow T_C = C \cdot G + T_A \quad \textbf{(2.11)}$$

$$C = \frac{T_{NOC} - 20}{800\,w/m^2} \quad \textbf{(2.12)}$$

Representation of circuit and result of A-300 SOLAR CELL of Sunpower© in Proteus are on same page in Figure 2.3. Proteus DC-Sweep is used to plot panel voltage and current for varying resistance $R19$ (Figure 2.3.a).

In Figure 2.3 used following Equations: Equation 2.1 for parameters of photovoltaic cell, Equation 2.2 for change temperature ambient to cell temperature, Equation 2.3 for parameters adjust to equivalent circuit and equation 2.4 to calculate variables to represented results on graphical depends to output measurement of equivalent circuit. The value of current source is calculate on variable I_L (current generate) on Equation 2.3 based on Equation 2.9, the value of current saturation on diode is calculate on variable I_0 on Equation2.3 based on Equation 2.10, the value of resistor series and parallel its calculate manually and indicate on Equation 2.3.

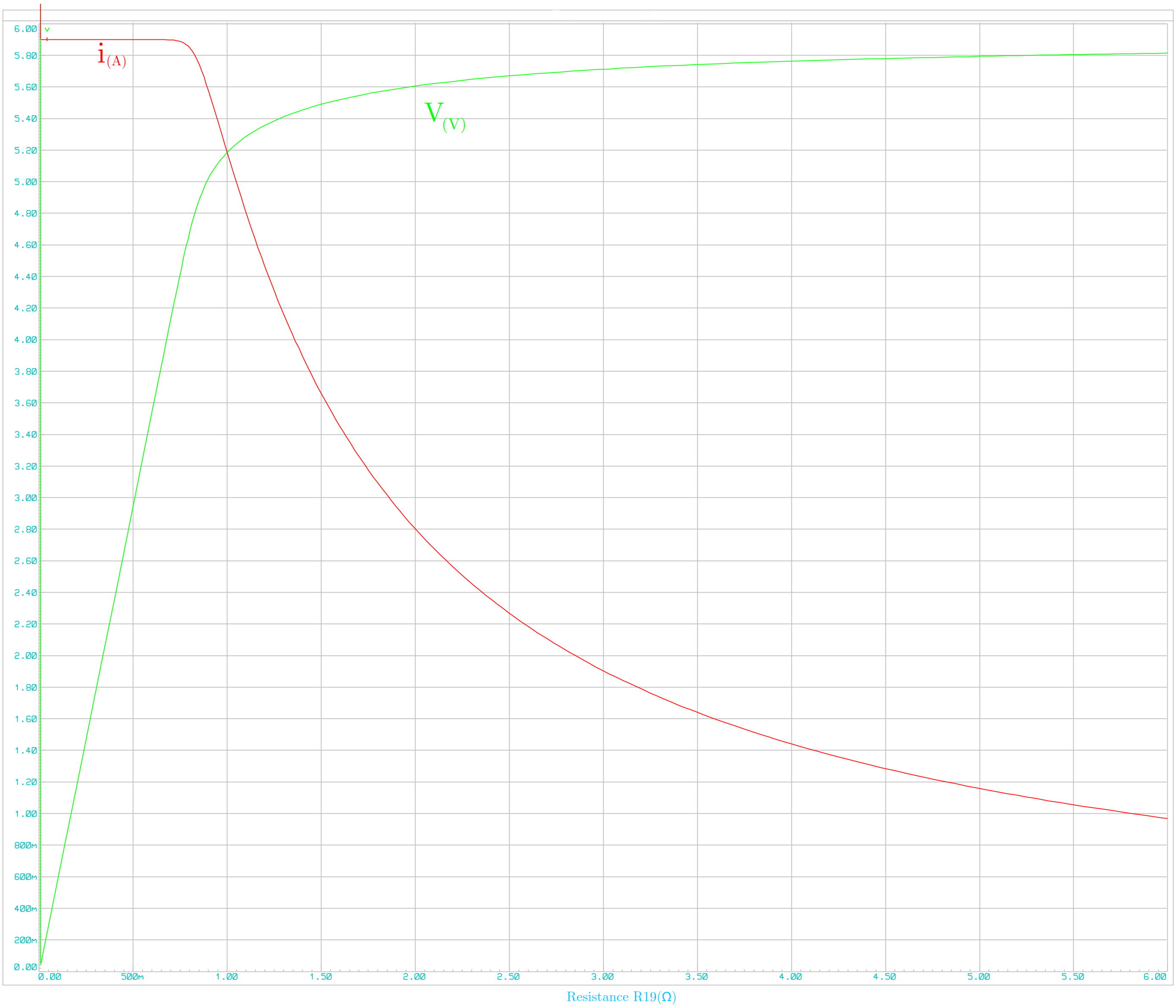

(a)

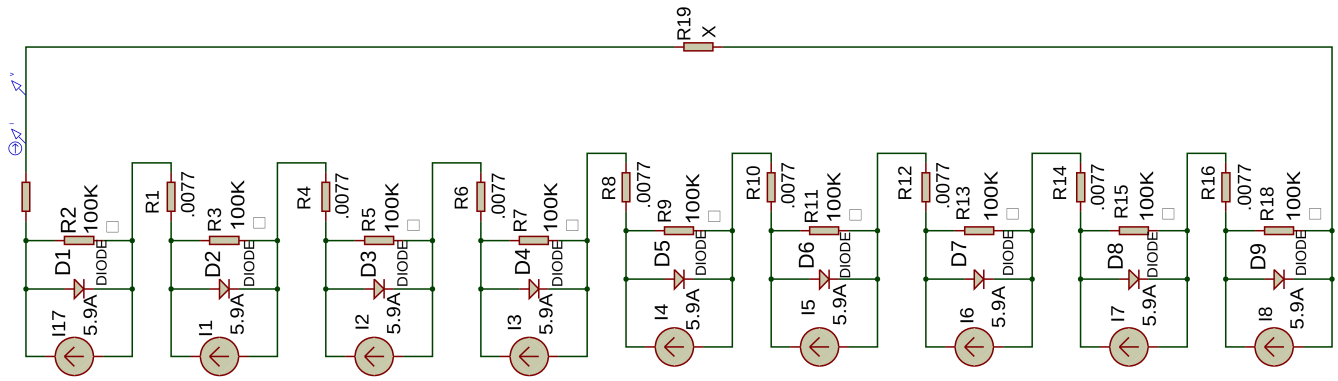

(b)

Figure 2.3: Photo voltaic panels modeling in Proteus.

By changing irradiation level, regarding to Equation 2.2, the current generated by PV cell will change.

Figure 2.3 represents panel IV characteristic for varying irradiation level (1000 W/m^2, 800 W/m^2 and 600 W/m^2) for the same value of cell temperature (25ºC).

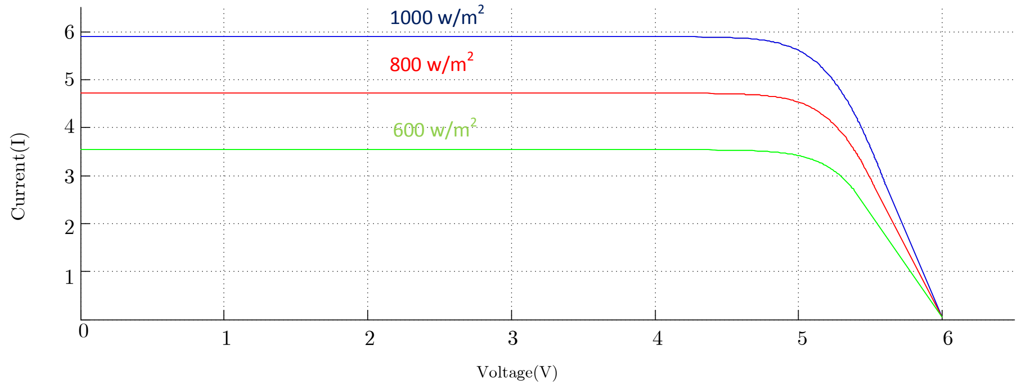

Figure 2.4: IV Curve for different values of irradiation.

3. CONFIGURATION OF SYSTEM

3.1 Introduction

Figure 3.1 illustrates a real-time implementation of a PV system using a microcontroller. This system consists of a PV panels connected in series, a boost converter to control the load voltage, a Atmega32 controller to implement the proposed MPPT algorithm,current sensor and a stand-alone resistive load.

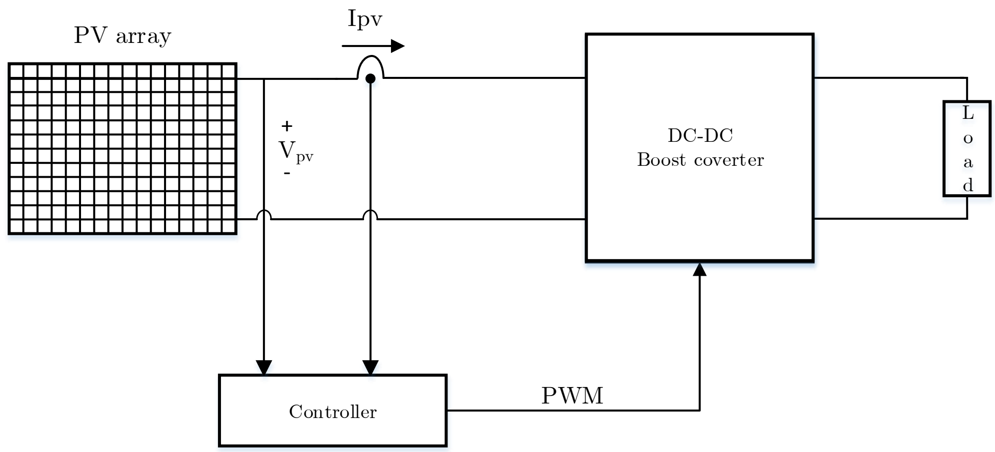

Figure 3.1: Configuration of a PV power control system.

In this configuration microcontroller by changing converter duty cycle optimizes output power of PV array.

3.2 Boost converter

The calculation are done by consider that converter operate at continues conduction mode.

The discontinues conduction mode arise when the switching ripple in an inductor current or capacitor voltage is large enough to cause the polarity of applied switch current or voltage to reverse, such that the current or voltage-unidirectional assumption made in realizing the switch with semiconductor devices are violated.

Before to start analysis of boost converter, understanding small ripple approximation is essential.

3.2.1 Small ripple approximation

It is impossible to build a perfect low-pass filter that allows the dc component to pass but completely removes the component at the switching frequency and its harmonics. So the low-pass filter must allow at least some small amount of the high-frequency harmonics generated by the switch to reach the output. Hence, in practice the output voltage waveform $v(t)$ appears as illustrated in Figure 3.2, and can be expressed as

$$v(t) = V + v_{ripple}(t) \tag{3.1}$$

so the actual output voltage $v(t)$ consist of the desired dc component V, plus small undesired ac component $v_{ripple}(t)$ arising from the incomplete attenuation of the switching harmonics by the low-pass filter. The magnitude of $v_{ripple}(t)$ has been exaggerated in Figure 3.2. The output voltage switching ripple should be small in any well-designed converter, since the object is to produce a dc output.
It is nearly always a good approximation to assume that magnitude of the switching ripple is much smaller than the dc component:

$$\|v_{ripple}\| \ll V \tag{3.2}$$

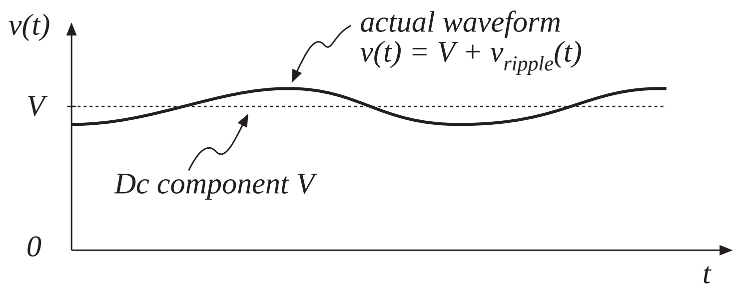

Figure 3.2: Output voltage waveform $v(t)$, consisting of dc component V and switching ripple $v_{ripple}(t)$ [1].

Therefore, the output voltage $v(t)$ is well approximated by its dc component V, with the small ripple term $v_{ripple}(t)$ neglected:

$$v(t) \approx V \tag{3.3}$$

This approximation, known as the small-ripple approximation, or the linear-ripple approximation, greatly simplifies the analysis of the converter waveforms [1].

3.2.2 Boost converter analysis

Boost converter is to connect a PV panel with a load in order to adjust the operating voltage and current of the PV panel at optimal values. A simplified diagram of a boost converter is illustrated in Figure 3.3.
A practical realizatioin of the switch, using a MOSFET and diode. Let us apply the small-ripple approximation and the principles of inductor current for this converter.

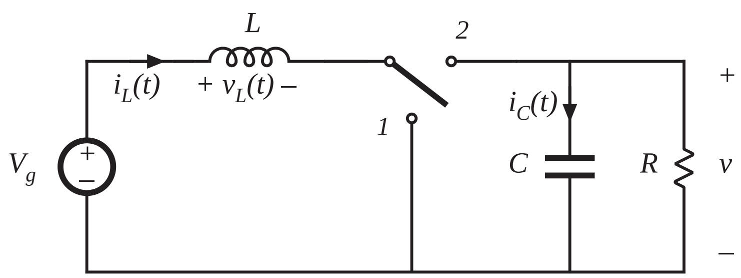

Figure 3.3: Boost converter with ideal switch [1].

With the switch in position 1, the right-hand side of inductor is connected to the ground, resulting in the network of Figure 3.4. The inductor voltage and capacitor current for this subinterval are given by

$$\begin{cases} v_L = V_g \\ i_C = -\dfrac{v}{R} \end{cases} \tag{3.4}$$

use of the linear ripple approximation, $v \approx V\ leads\ to$

$$\begin{cases} v_L = V_g \\ i_C = -\dfrac{V}{R} \end{cases} \tag{3.5}$$

with the switch on position 2, the inductor is connected to the output, leading to the circuit of Figure 3.5. The inductor voltage and capacitor current are then

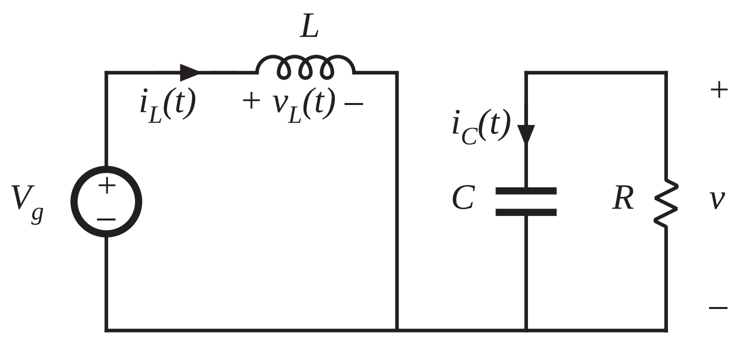

Figure 3.4: Boost converter circuit while switch in position 1 [1].

$$\begin{cases} v_L = V_g - v \\ i_C = i_L - \dfrac{v}{R} \end{cases} \tag{3.6}$$

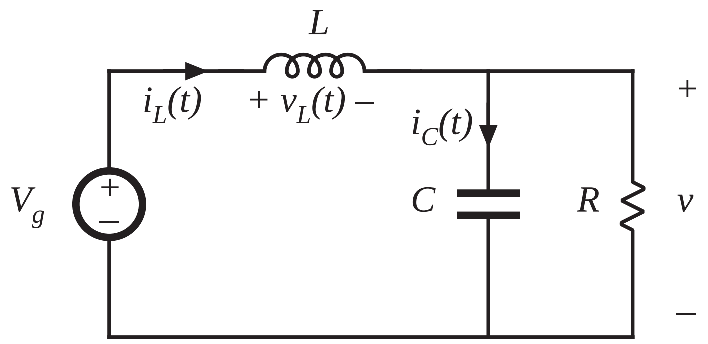

Figure 3.5: Boost converter circuit while switch in position 2 [1].

Use of the small-ripple approximation , $v \approx \mathrm{V}$ *and* $\mathrm{i}_L = I$, leads to

$$\begin{cases} v_L = V_g - V \\ i_C = I - \dfrac{V}{R} \end{cases} \tag{3.7}$$

Equation (3.5) *and* (3.7) are used to sketch the inductor voltage and capacitor current waveform of Figure 3.6.

It can be inferred from the inductor voltage waveform of Figure 3.6 that the dc output voltage V is greater than the input voltage V_g. During the first subinterval, $v_L(t)$ is equal to the dc input voltage V_g, over one switching period must be zero, negative volt-seconds must be applied during the second subinterval. Therefore, the inductor voltage during the the second subinterval, $(V_g - V$, must be negative. Hence V is grater than V_g. The total volt-seconds applied to the inductor over one switching period are :

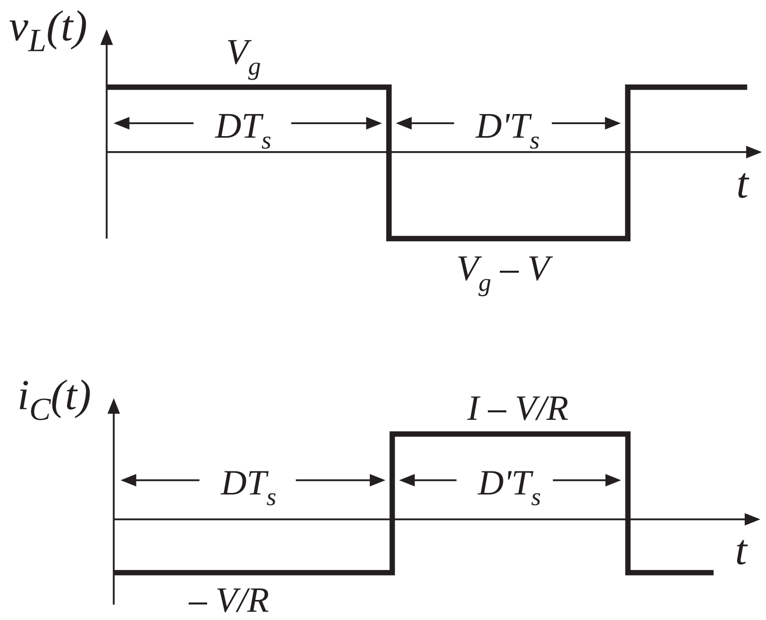

Figure 3.6: Boost converter voltage and current waveform [1].

$$\int_0^T v_{(L)} dt = (V_g) DT_s + (V_g - V) D'T_s \quad \textbf{(3.8)}$$

By equation this expression to zero and collecting terms, one obtains

$$V_g \left(D + D'\right) - VD' = 0 \quad \textbf{(3.9)}$$

Solution for V, and by noting that $(D + D') = 1$, yields the expression for output voltage,

$$V = \frac{V_g}{D'} \quad \textbf{(3.10)}$$

The voltage conversion ratio $M(D)$ is the ratio of the output to the input voltage of a dc-dc converter.

Equation 3.10 predicts that the voltage conversion ratio is given by

$$M(D) = \frac{V}{V_g} = \frac{1}{D'} = \frac{1}{1 - D} \quad \textbf{(3.11)}$$

So the ideal boost converter is capable of producing output voltage greater than input voltage. There are, of course, limits to the output voltage that can be produced by a practical boost converter. The dc component of the inductor current is derived by use of the principle of capacitor charge balanced. The net change in capacitor charge over one switching period is found by integrating the $i_C(t)$ waveform of Figure 3.6.

$$\int_0^{T_s} i_c(t)\,dt = \left(-\frac{V}{R}\right) DT_s + \left(I - \frac{V}{R}\right) D'T_s \quad \textbf{(3.12)}$$

Collecting terms, and equating the result to zero, leads the steady-state result

$$I = \frac{V_g}{D'^2 R} \quad \textbf{(3.13)}$$

We sketch inductor current $i_L(t)$ waveform and derive an expression for the inductor current ripple Δi_L. The inductor voltage waveform $v_L(t)$ has been already found Figure 3.6, so we can sketch the inductor current waveform directly. During the first subinterval, with the switch in position 1, the slope of the inductor current is given by

$$\frac{di_L(t)}{dt} = \frac{v_L(t)}{L} = \frac{V_g}{L} \quad \textbf{(3.14)}$$

Likewise, when the switch is in position 2, the slope of the inductor current waveform is

$$\frac{di_L(t)}{dt} = \frac{v_L(t)}{L} = \frac{V_g - V}{L} \quad \textbf{(3.15)}$$

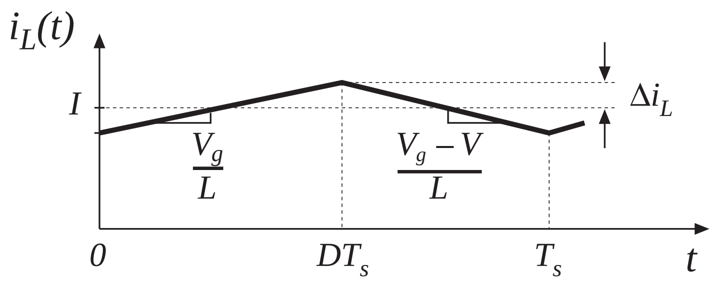

Figure 3.7: Boost converter inductor current waveform $i_L(t)$ [1].

The inductor current waveform is sketched in Figure 3.7. During the first subinterval, the change in indutor current $2\Delta i_L$, is equal to the slope multiplied by the length of the subinterval or

$$2\Delta i_L = \frac{V_g}{L} DT_s \quad \textbf{(3.16)}$$

solution for Δi_L leads to

$$\Delta i_L = \frac{V_g}{2L} DT_s \tag{3.17}$$

This expression can be used to select the inductor value L such that a given value of Δi_L is obtained.

Likewise, the capacitor voltage $v(t)$ waveform can be sketched, and an expression derived for the output voltage ripple peak magnitude Δv. The capacitor current waveform $i_C(t)$ is given in Figure 3.6.

During first subinterval, the slope of the capacitor voltage $v(t)$ is

$$\frac{dv_c(t)}{dt} = \frac{i_C(t)}{C} = \frac{-V}{RC} \tag{3.18}$$

During second subinterval, the slope is

$$\frac{dv_c(t)}{dt} = \frac{i_C(t)}{C} = \frac{I}{C} - \frac{V}{RC} \tag{3.19}$$

The capacitor voltage waveform is sketched in Figure 3.8. During the first subinterval, the change in capacitor voltage, -2Δv, is equal to the slope multiplied by the length of the subinterval:

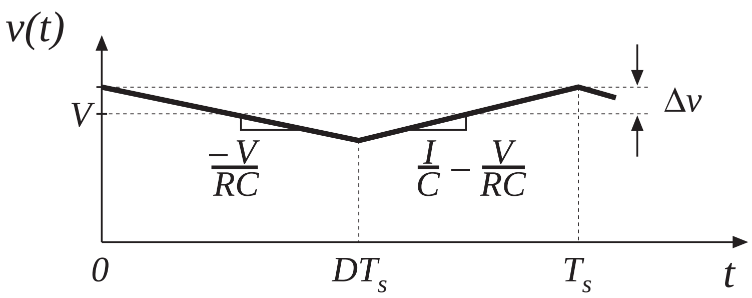

Figure 3.8: Boost converter output voltage waveform $v(t)$ [1].

$$-2\Delta v = \frac{-V}{RC} DT_s \tag{3.20}$$

solution for Δv yields

$$\Delta v = \frac{V}{2RC} DT_s \tag{3.21}$$

This expression can be used to select the capacitor value C to obtain a given output voltage ripple peak magnitude Δv [1].

Thus the selection of boost converter components (the input inductor and the output capacitor) is a compromise between dynamic responses and the MPPT algorithm trigger time. The maximum value of the state variables should be calculated to estimate the value of the boost converter. The specifications of the boost converter are summarize in Table 3.1 and the calculated parameters of are listed in Table 3.2

Table 3.1: Specifications of the boost converter.

Parameter	Symbol	Value	Unit
Switching frequency	f_{sw}	32.0	kHz
Maximum input voltage	$V_{pv(max)}$	6.03	V
Rated inductor current	I_L	5.54	A
Maximum voltage ripple	$V_{ripple(max)}$	1.2	V

Table 3.2: Parameters of the boost converter.

Parameter	Symbol	Value	Unit
Minimum duty cycle	D_{min}	0	%
Maximum duty cycle	D_{max}	80	%
Minimum inductance	L_{min}	47	μH
Peak inductor current	$I_{L(pk)}$	6.3	A
Minimum capacitance	C_{min}	80	μF

3.3 Algorithm for maximum power point tracking

For understanding optimize array power with PSO algorithm we must be familiar with this algorithm so this optimize method is introduced briefly.

3.3.1 Particle Swarm Optimization method

3.3.1.1 Introduction

Particle swarm optimization (PSO) is originally attributed to Kennedy, Eberhart and Shi was first intended for simulating social behavior. The book by Kennedy and Eberhart describes many philosophical aspects of PSO and swarm intelligence. An extensive survey of PSO applications is made by Poli. PSO is a metaheuristic as it makes few or no assumptions about the problem being optimized and can search very large spaces of candidate solutions. PSO does not use the gradient of the problem being optimized, which means PSO does not require that the optimization problem be differentiable as is required by classic optimization methods such as gradient descent and quasi-newton methods. A basic variant of the PSO algorithm works by having a population (called a swarm) of candidate solutions (called particles). These particles are moved around in the search-space according to a few simple formulae. The movements of the particles are guided by their own best known position in the search-space as well as the entire swarm's best known position. When improved positions are being discovered these will then come to guide the movements of the swarm. The process is repeated and by doing so it is hoped, but not guaranteed, that a satisfactory solution will eventually be discovered [2].

3.3.1.2 Mathematical modelig of Particle Swarm Optimization

Consider an optimization problem of D variables. A swarm of N particles is initialized in which each particle is assigned a random position in the D-dimensional hyperspace such that each particle's position corresponds to a candidate solution for the optimization problem. Let x denote a particle's position (coordinate) and v denote the particle's flight velocity over a solution space. Each individual x in the swarm is scored using a scoring function that obtains a score (fitness value) representing how good it solves the problem. The best previous position of a particle is P$best$. The index of the best particle among all particles in the swarm is G$best$. Each particle records its own personal best position (P$best$), and knows the best positions found by all particles in the swarm (G$best$). Then, all particles that fly over the D-dimensional solution space are subject to updated rules for new positions, until the global optimal position is found. Velocity and position of a particle are updated by the following stochastic and deterministic update rules:

$$v_i^{k+1} = wv_i^k + c_1 Rand() \times (Pbest_i^k - x_i^k) + c_2 Rand() \times (Gbest^k - x_i^k) \qquad \textbf{(3.22)}$$

$$x_i^{k+1} = x_i^k + v_i^{k+1} \qquad \textbf{(3.23)}$$

where w is an inertia weight, c_1 and c_2 are acceleration constants, and Rand( ) is a random number between 0 and 1. Equation 3.22 indicates that the velocity of a particle is modified according to three components. The first component is its previous velocity, v_i^k , scaled by an inertia, w. This component is often known as "habitual behavior". The second component is a linear attraction toward its previous best position, $Pbest_i^k$, scaled by the product of an acceleration constant, c_1, and a random number. Note that a different random number is assigned for each dimension. This component is often known as "memory" or "self-knowledge". The third component is a linear attraction toward the global best position, $Gbest^k$, scaled by the product of an acceleration constant, c_2, and a random number. This component is often known as "team work" or "social knowledge."

Figure 3.9 illustrates a search mechanism of a PSO technique using the velocity update rule 3.22 and the position update rule 3.23.

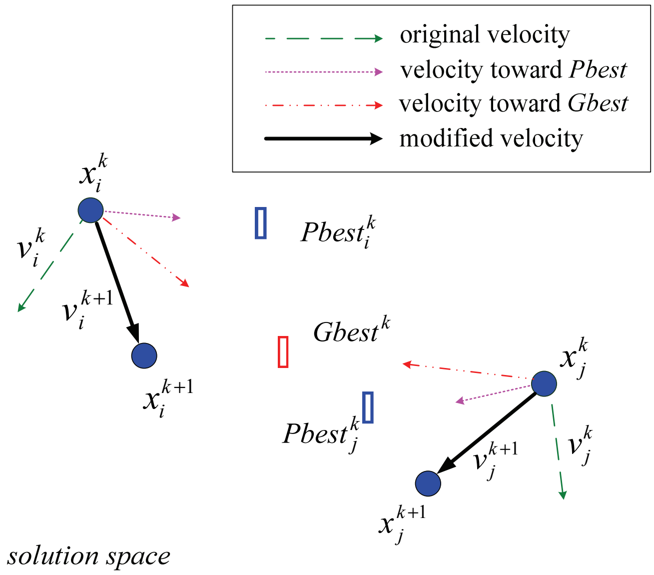

Figure 3.9: Searching mechanism of a PSO [2].

Acceleration constants c_1 and c_2 represent the weights of the stochastic acceleration terms that push a particle toward $Pbest$ and $Gbest$, respectively. Small values allow a particle to roam far from target regions. Conversely, large values result in the abrupt movement of particles toward target regions. Suitable correction of inertia w in Equation 3.22 provides a balance between global and local explorations, thereby reducing the number of iterations when finding a sufficiently optimal solution [2].

3.3.2 How use microcontroller to track maximum power point

The procedure of the MPPT using PSO algorithm is presented in the flowchart shown in Figure 3.10.

1. Determine number of swarm and number of iteration (stopping criteria is the number of iteration) and global Watt by 0 value.
2. initialize swarm position by the random number between 0 and 100 (swarm are duty cycle which select randomly by random function in microcontroller and this value is buck converter operate duty cycle) and swarm velocity by zero value.
3. Evaluation of the objective function of the corresponding initialized particles. The objective function is chosen to be wattmeter value which microcontroller read in A/D pins and in initialize part we name it best cost because in initialize level the first value is the best value.
4. If the best value of particle is greater than global cost (watt) go to level 5 else go to level 6.
5. Write particle position and cost to global cost and position.
6. Go to next particle by increasing i value.
7. If i is greater than i_{max} go to step 8 else go to 1.
8. Choose first particle (i=1).
9. Updating particle position and velocity according Equation 3.22 and Equation 3.23.
10. Calculate particle cost (wattmeter value).
11. If particle cost is greater than particle best cost go to step 12 else go to 15.
12. Write particle cost and position to particle best position and cost.
13. If particle cost is greater than global cost go to 14.
14. Write particle position to global position and particle cost to global cost.

15. Go to next particle.
16. If i is greater than i_{max} go to 17 else go to 9.
17. Go to next iteration and start from first particle.
18. If iteration is greater than maximum iteration go to 19 else go to 9.
19. Microcontroller operate at global duty cycle for 10 seconds and go to step 1.

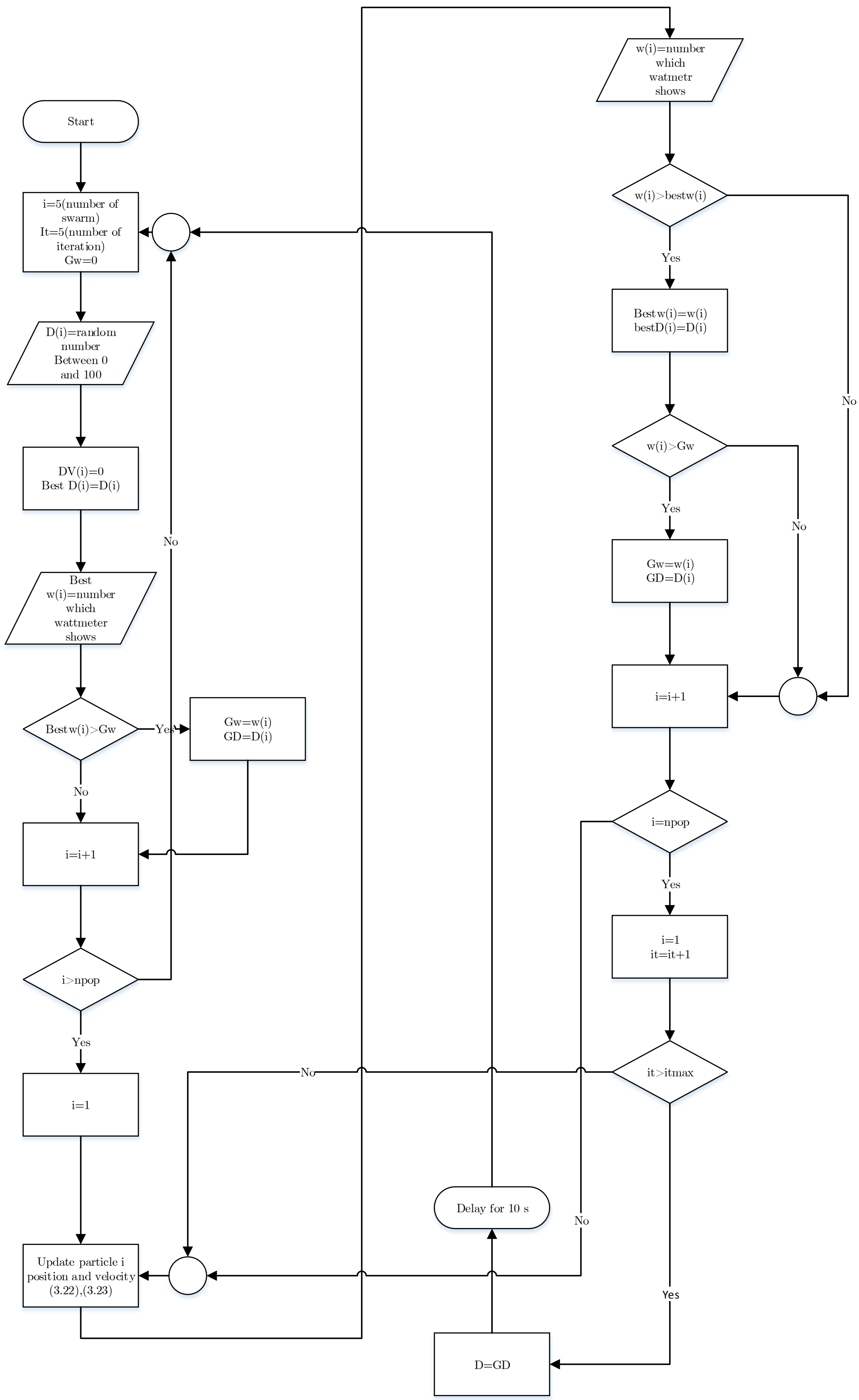

Figure 3.10: Flowchart of searching algorithm of PSO.

4. SIMULATION RESULTS

Following Chapter 2 solar panel is modeled in Proteus. Also CodevisionAVR is used for programming ATmega32 microcontroller. The schematic circuit is represented in Figure 4.1.

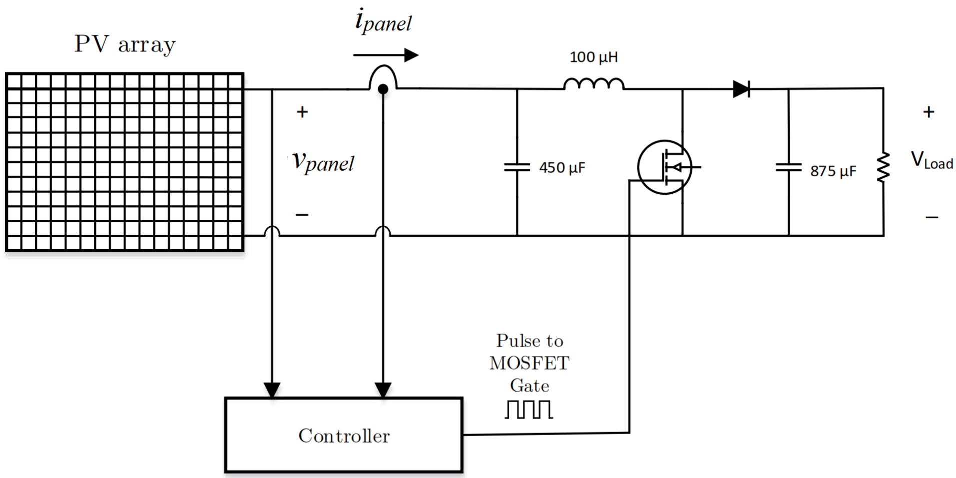

Figure 4.1: Schematic circuit of panel and controller.

In Figure 4.2 the simulation result for unchanged ambient condition, is shown, running time is 1 second.

As shown in Figure 3.10 the algorithm restart every 10 second but for simulation purpose it is considered the delay time is 1 second. Following Figure 4.3 when irradiation changes at 0.8^{th} second, the panel power is lower than desired value, but when new searching cycle starts, the panel operates at maximum power point (When irradiation change from 1000 to 600 $watt/m^2$ maximum power also change from 28.1 to 17 Watt).

To check controller operation by different load value, the load is changed from 4 to 2Ω *in* 0.8^{th} second.

As shown in Figure 4.4, when the load changes, the panel does not operate at maximum power, until new cycle starts to search maximum power point and panel track exactly maximum power point again.

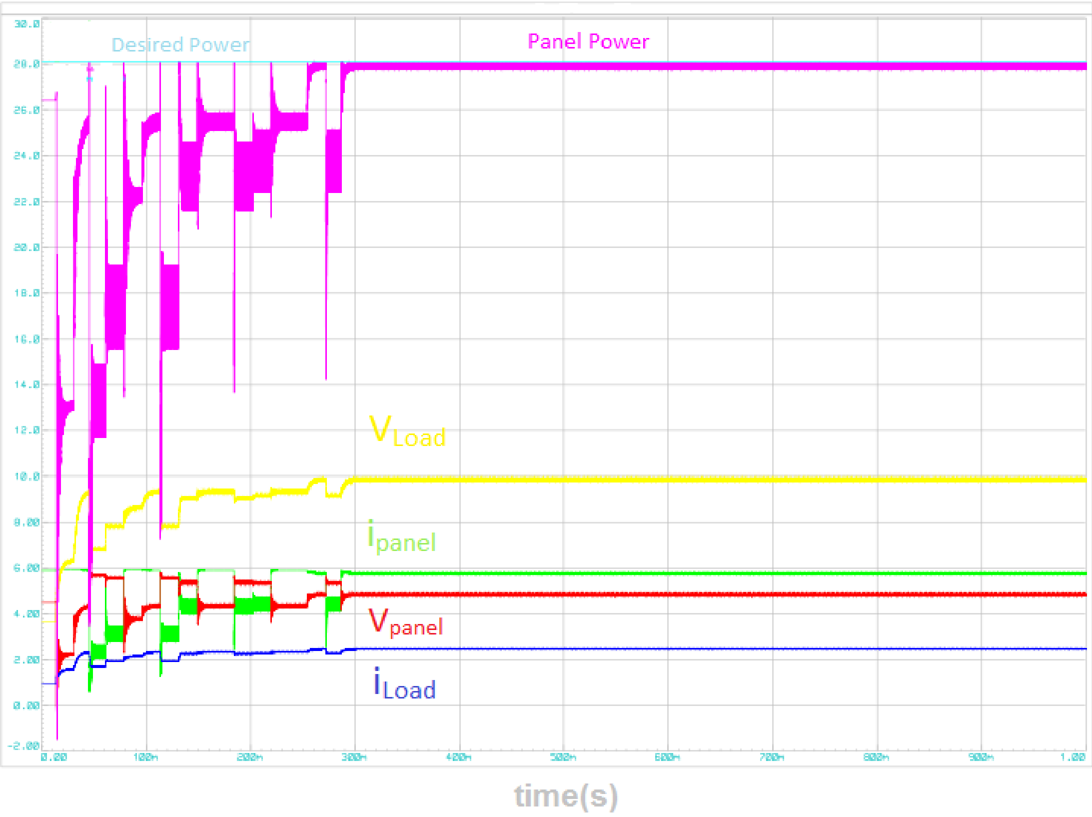

Figure 4.2: Simulation results.

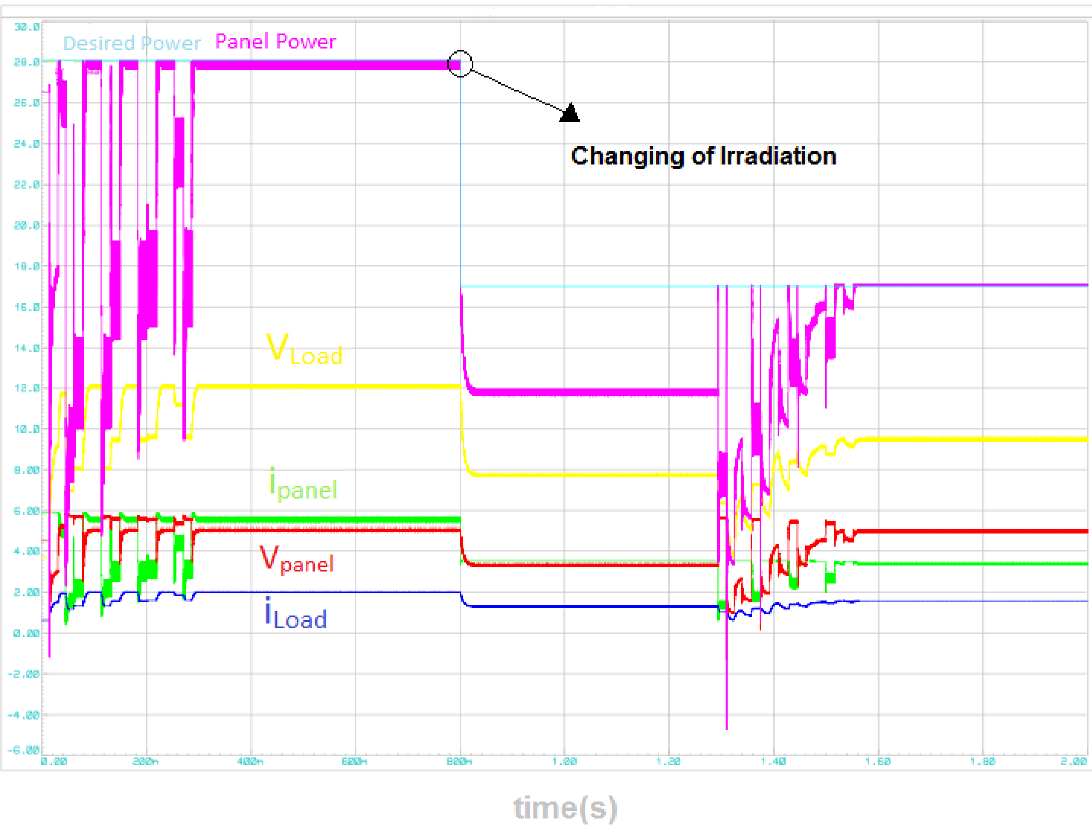

Figure 4.3: Simulation results when irradiation changes.

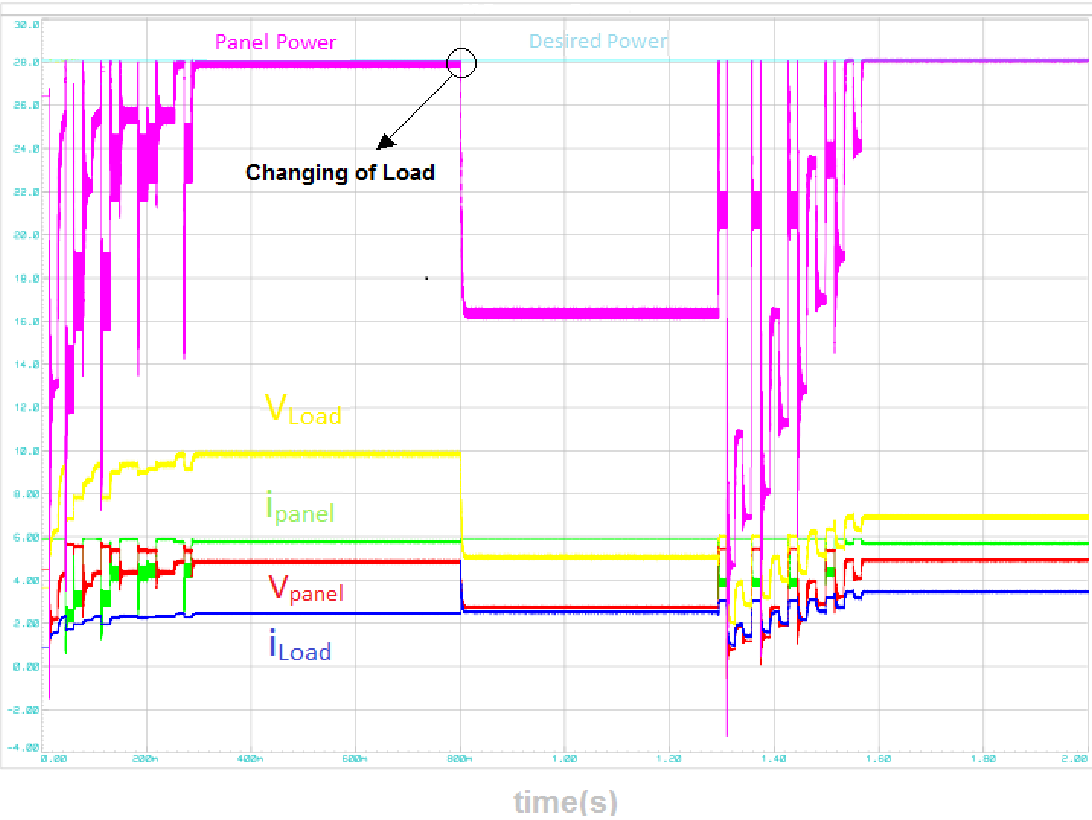

Figure 4.4: Simulation results when load changes.

5. EXPERIMENTAL RESULTS AND ANALYSIS

An experiment is conducted to verify the performance of the MPPT algorithm are implemented with AVR microcontroller . The PV panels output current i_{pv} is sensed with current sensor and voltage v_{pv} is sensed by microcontroller and this data are processed by microcontroller system, then PWM pulse are outputted to driving circuit of the boost converter. So fully digital control is realized.

5.1 Experimental Setup

From MPPT system diagram which is shown in 5.1 we can see that the system is comprised of three parts, PV Panels, Boost Converter, and the MPPT controller.

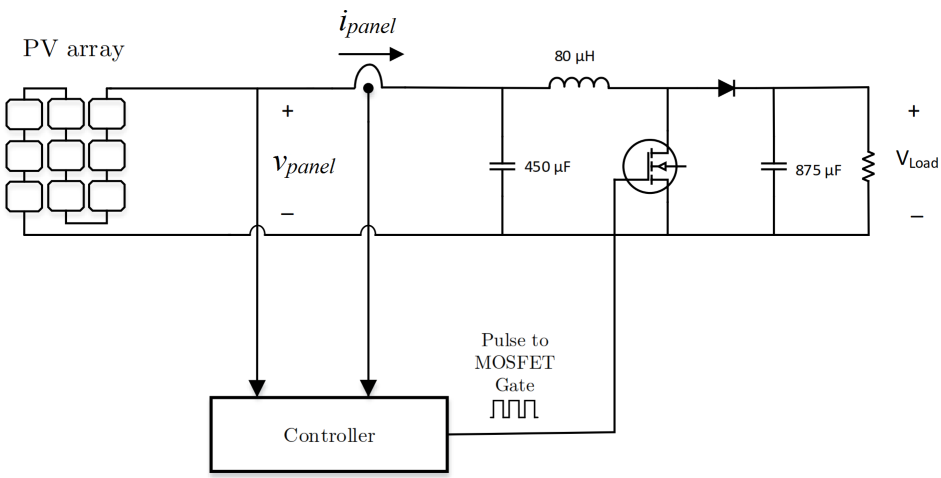

Figure 5.1: Experimental schematic circuit of panel and controller.

5.1.1 PV Panels

A PV panel manufactured by Sunpower©is used in the in the experiment [Appendix B 2.1].

Each module has the following parameters under standard test condition of 1000W/m^2, 25°C cell temperature. In the experiment, 9 module are series.

The open circuit voltage(V_{OC}) is 0.670V.

The short-circuit current (I_{SC}) is 5.9A.
The voltage at the MPP(V_{MPP}) is 0.560V.
The current at the MPP(I_{MPP}) is 5.14A.

5.1.2 The MPPT Converter

In the MPPT system implemented for simplicity variable resistor load is used. By consider section 3.2.2 , the component of converter are determined.

5.1.2.1 MOSFET Rating

The maximum current that the power switch carries is the PV short-circuit current, I_{SC}. For high reliability, the rated current of MOSFET should be $1.2 \sim 1.5\mathrm{I}_{SC}$, which is $5.9 \times 1.5 = 8.85A$.
The maximum voltage that the switch standard is output voltage of boost converter v_{out}. For high reliability, the rated voltage of MOSFET should be $1.5V_{out}$, which is $12 \times 1.5 = 18V$.
By consider this calculation and available component in laboratory IRFP150 was chosen [Appendix B 2.2].

5.1.2.2 Diode Rating

The maximum current that the diode carries is also I_{SC}. For high reliability, the rated current of the diode should also be $1.2 \sim 1.5$ which also is 8.85A.
The maximum voltage that the diode blocks is V_{out}. For high reliability, the rated voltage of diode should be $1.5V_{out}$, which is 18V.
Similarly consideration for diode cause MUR805G was selected [Appendix B 2.3].

5.1.3 Sensor

5.1.3.1 Current Sensor

Because microcontroller does not have current sensor, LTS25 NP current transducer is used to sense current and turn it to voltage form to microcontroller process [Appendix B 2.6]. There is linear relation between sensed current and output voltage, this voltage swing above 2.5v, it means when current is zero (open-voltage) the output voltage is 2.5v and when the current is in opposite direction the voltage is lower than this value.

5.1.4 Controller

5.1.4.1 Microcontroller

The controller which is used in this thesis is AVR ATMEGA 32 which is production of ATMEL company [Appendix B 2.4]. The microcontroller system sample the PV panels output current i_{pv} (with current sensor) and voltage v_{pv} by A/D converters, then processes them and output the PWM signals to the driving circuit of the boost converter by the I/O unit.

5.1.4.2 MOSFET Driver

The switching signal for a transistor is usually generated by a logic circuit or a microcontroller, which provides an output signal that typically is limited to a few milliamperes of current. Consequently, a transistor which is directly driven by such a signal would switch very slowly, with correspondingly high power loss. During switching, the gate capacitor of the transistor may draw current so quickly that it causes a current overdraw in the logic circuit or microcontroller, causing overheating which leads to permanent damage or even complete destruction of the chip. To prevent this from happening, a gate driver is provided between the microcontroller output signal and the power transistor. By consider the selected MOSFET and microcontroller, TLP250 by Toshiba is used to run MOSFET [Appendix B 2.5].

5.2 Experimental Results

In experimental by consider ambient condition and in unchanged irradiation level and temperature and fix wind speed, panel IV curve is drawn in Figure 5.2.a.

In Figure 5.2.b it can be seen by changing voltage how panel power change, the maximum power point voltage is 4.6V.

This results are calculated in unchanged ambient condition with variable resistor load which connected to solar panel, and by changing load resistance voltage and current of panel change, and by record this data, they are plotted.

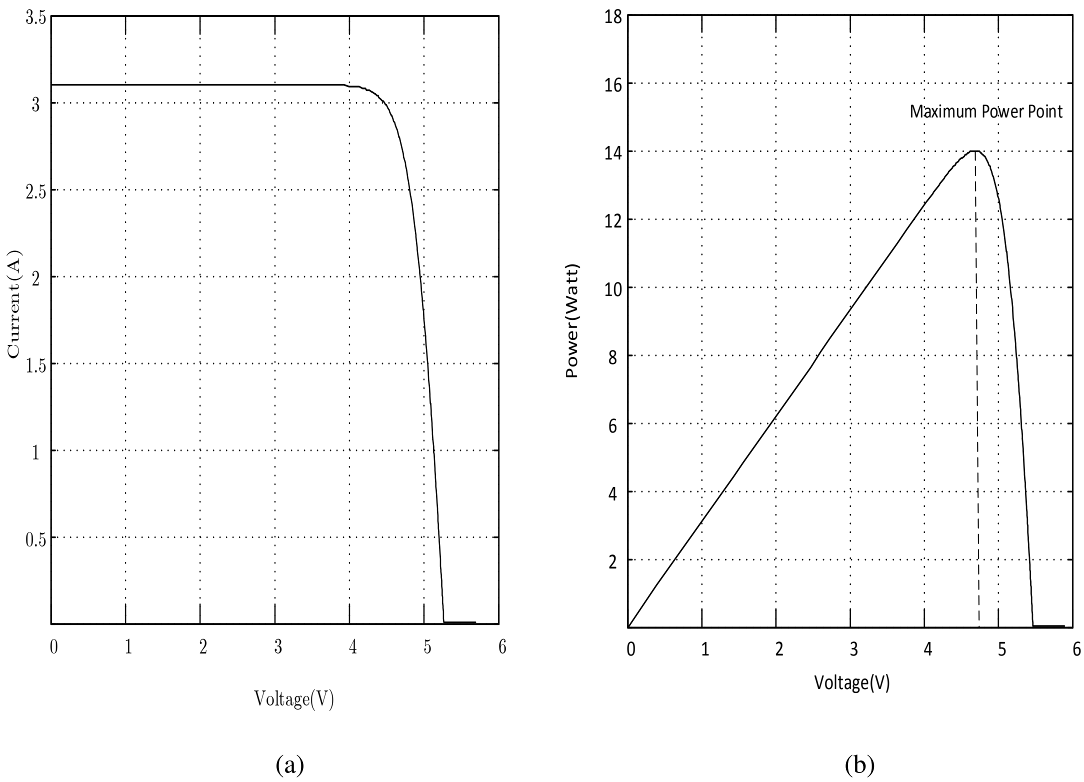

Figure 5.2: Real panel characteristic a) *IV* and b) *PV* curve at 2015.4.23 2:20pm.

Implemented microcontroller by changing boost converter duty cycle, changes panel output voltage, and track maximum point voltage in Figure 5.3, the experimental results are for 100s as mentioned in Section 3.3.2, this algorithm start to search new optimum point in every seconds which can change for different condition rely on some factor like how fast shadow irradiation change, temperature and wind speed but the it most rely on shadow changing. By considering university laboratory condition, delay time for restart algorithm is 10 second.

The result in Figure 5.3, is for 50s and control system in 5 searching for optimal point , track almost same voltage value because ambient condition unchanged in experiment period and it adopt with simulation section. For simplicity the resistor load is used.
To obtain function of controller in load changing condition , as shown in Figure 5.4 at about 60^{th} second the load is changed from 12Ω to 8Ω , at this condition voltage drop from 4.6V (optimal point) to 3.9V, and panel operate at this volt until after seconds, controller start to search new duty cycle which cause to converter operate at optimal voltage .

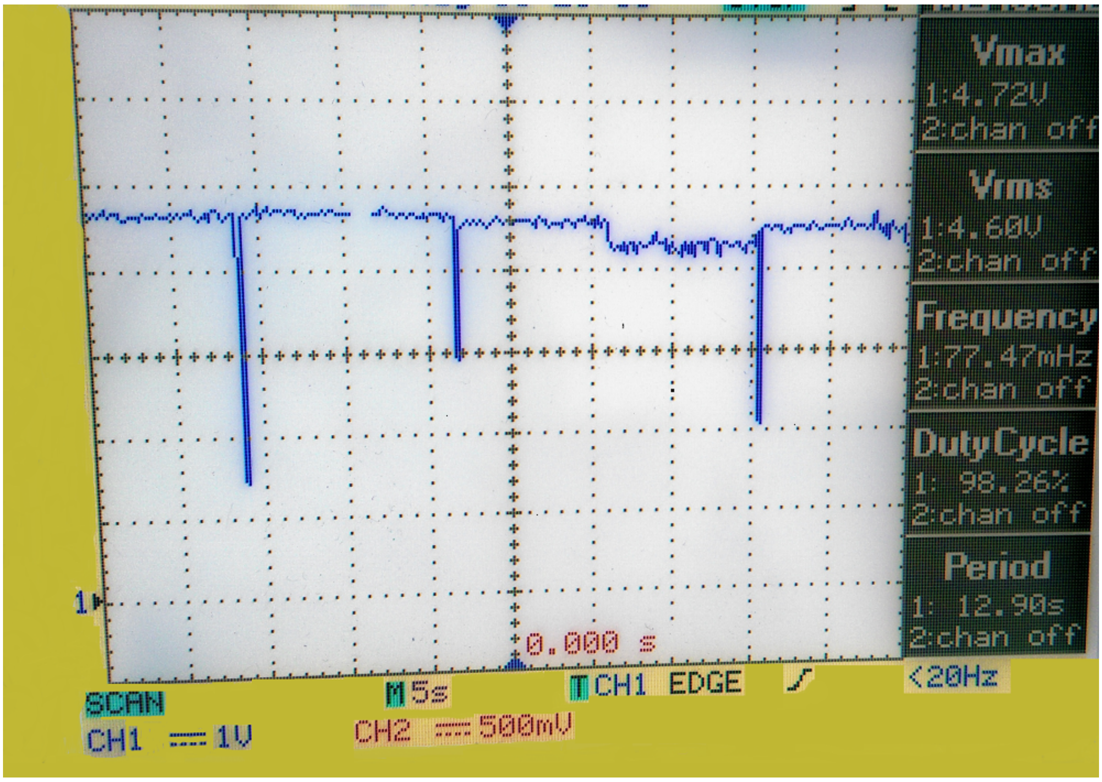

Figure 5.3: Experimental result of MPPT technique in unchanged irradiation and temperature condition.

As it is shown in Figure 5.4 about 70^{th} second, by new duty cycle converter back to desired voltage.

The other scenario which must discuss and adopt with simulation part is operation of panel and controller in different irradiation level. Because this experiment is done in different day of other two experiment, the maximum voltage in full irradiance is calculated with same procedure is 4.9V and when irradiance decrease, new optimal point is 4.6V.

As shown in Figure 5.5, about 5^{th} second the irradiation decrease and results panel operate in 4V which is not optimal point for new irradiation level, as in about 10^{th} second controller search new optimal point, and operate at new optimal point.

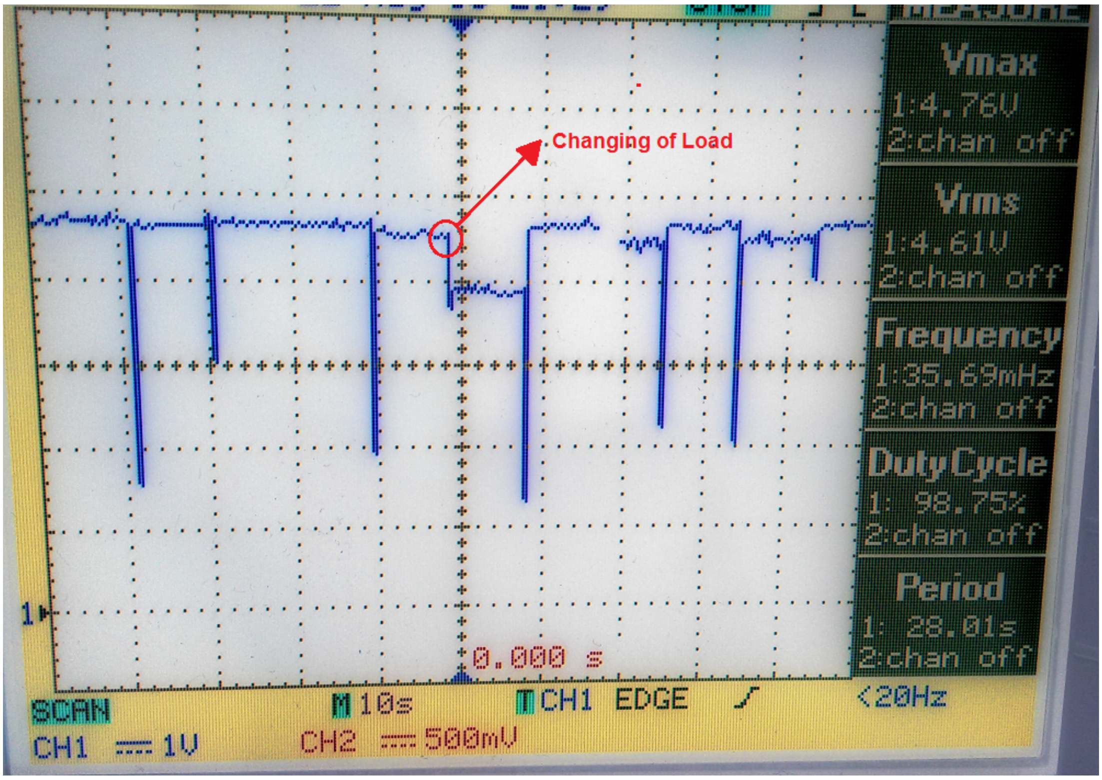

Figure 5.4: Experimental results of panel voltage load change from 12Ω to 8Ω.

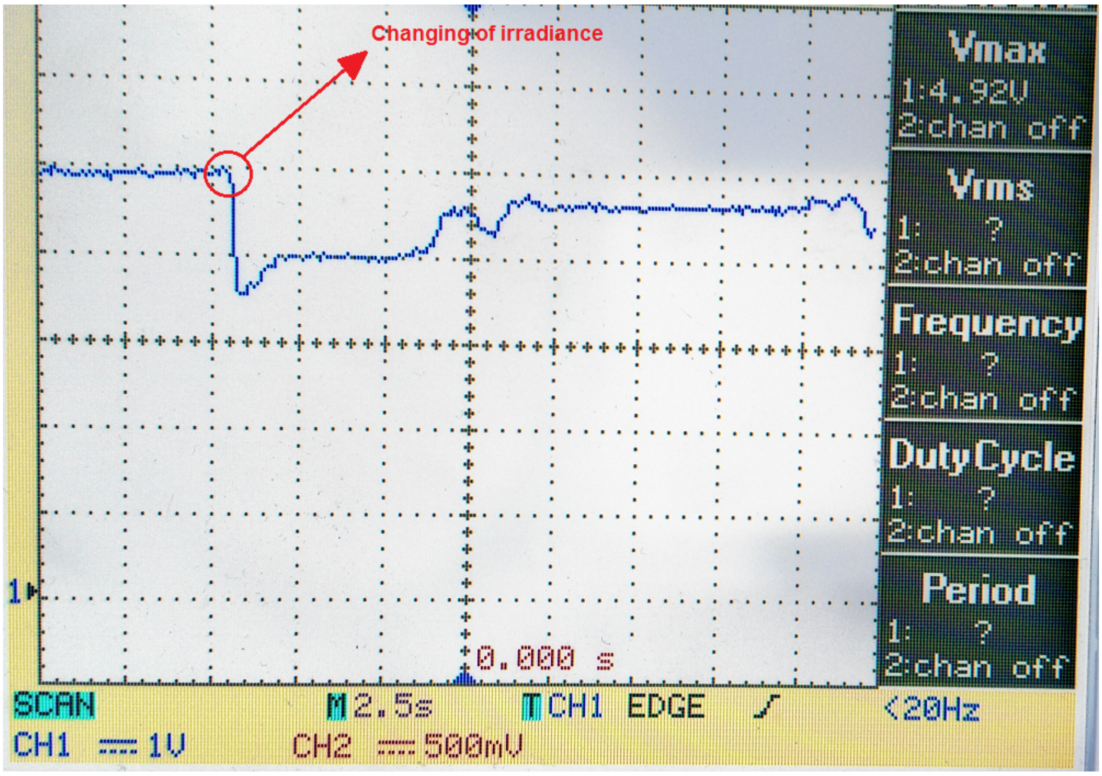

Figure 5.5: Experimental result of panel voltage with irradiation change.

6. CONCLUSIONS AND FUTURE WORK

In this algorithm which base on PO method we just need a current sensor microcontroller (we use AVR ATmega32) and boost converter. One of the important specification of PSO algorithm is tracking global maximum point even in presence of multiple local maximums.

Compared to other method which use microcontroller like look table-up method, this method does not need any information about panel and environment condition i.e, we can use this controller for any panel in any condition also changing of temperature and irradiation does not affect operation.

This method does not need any control loop so it is low cost, which does process with avr microcontroller and current sensor. By comparing this algorithm with other intelligent systems like fuzzy controller or neural network system this algorithm is more simple.

Periodically search can be disadvantage of this method, in another word, when the ambient condition or load change the controller does not track maximum point, until search mechanism starts to find new optimum point. This feature can be corrected by periodically replacing searching by another method.

conditional search method can be investigated as a future work. By using this method controller calculate output power and if it changes in large value, controller start to search new optimal point, but there must be some consideration because instant shadowing can affect this feature too and panel periodically tune at maximum point.

REFERENCES

[1] **Erickson, R.W. and Maksimovic, D.** (2001). *Fundamentals of power electronics*, Springer Science & Business Media.

[2] **Lazinica, A.** (2009). *Particle swarm optimization*, InTech Kirchengasse.

[3] **Esram, T. and Chapman, P.** (2007). Comparison of Photovoltaic Array Maximum Power Point Tracking Techniques, *IEEE Transactions on Energy Conversion*, ***22***(2), pp.439–449.

[4] **Liu, F.**, **Kang, Y.**, **Zhang, Y. and Duan, S.** (2008). Comparison of P&O and hill climbing MPPT methods for grid-connected PV converter, *3rd IEEE Conference on Industrial Electronics and Applications, 2008. ICIEA 2008.*, IEEE, pp.804–807.

[5] **Natasha, N.**, **Bhuiyan, W. and Razzak, M.** (2014). Implementation of Maximum Power Point Tracking in a photovoltaic inverter using Incremental Conductance technique, *International Conference on Electrical and Computer Engineering (ICECE), 2014*, pp.329–332.

[6] **Kuo, Y.C.**, **Liang, T.J. and Chen, J.F.** (2001). Novel maximum-power-point-tracking controller for photovoltaic energy conversion system, *IEEE Transactions on Industrial Electronics*, ***48***(3), pp.594–601.

[7] **Kobayashi, K.**, **Matsuo, H. and Sekine, Y.** (2004). A novel optimum operating point tracker of the solar cell power supply system, *IEEE 35th Annual Power Electronics Specialists Conference, 2004. PESC 04. 2004*, volume 3, pp.2147–2151.

[8] **Masoum, M.**, **Dehbonei, H. and Fuchs, E.** (2002). Theoretical and experimental analyses of photovoltaic systems with voltageand current-based maximum power-point tracking, *IEEE Transactions on Energy Conversion,*, ***17***(4), pp.514–522.

[9] **Noguchi, T.**, **Togashi, S. and Nakamoto, R.** (2002). Short-current pulse-based maximum-power-point tracking method for multiple photovoltaic-and-converter module system, *IEEE Transactions on Industrial Electronics,*, ***49***(1), pp.217–223.

[10] **El-Telbany, M.**, **Mahgoub, A. and Zekry, A.** (2014). An intelligent fuzzy controller for maximum power point tracking, *Computer Engineering Conference (ICENCO), 2014 10th International*, pp.107–111.

[11] **Hiyama, T.**, **Kouzuma, S. and Imakubo, T.** (1995). Identification of optimal operating point of PV modules using neural network for real time maximum power tracking control, *IEEE Transactions on Energy Conversion,*, ***10***(2), pp.360–367.

[12] **Midya, P.**, **Krein, P.**, **Turnbull, R.**, **Reppa, R. and Kimball, J.** (1996). Dynamic maximum power point tracker for photovoltaic applications, *27th Annual IEEE Power Electronics Specialists Conference, 1996. PESC '96 Record.*, volume 2, pp.1710–1716.

[13] **Bodur, M. and Ermis, M.** (1994). Maximum power point tracking for low power photovoltaic solar panels, *Electrotechnical Conference, 1994. Proceedings., 7th Mediterranean*, volume 2, pp.758–761.

[14] **Kitano, T.**, **Matsui, M. and hong Xu, D.** (2001). Power sensor-less MPPT control scheme utilizing power balance at DC link-system design to ensure stability and response, *The 27th Annual Conference of the IEEE Industrial Electronics Society, 2001. IECON '01.*, volume 2, pp.1309–1314.

[15] **Arias, J.**, **Linera, F.**, **Martin-Ramos, J.**, **Pernia, A. and Cambronero, J.** (2004). A modular PV regulator based on microcontroller with maximum power point tracking, *Industry Applications Conference, 2004. 39th IAS Annual Meeting. Conference Record of the 2004 IEEE*, volume 2, pp.1178–1184.

[16] **Bhide, R. and Bhat, S.** (1992). Modular power conditioning unit for photovoltaic applications, *23rd Annual IEEE Power Electronics Specialists Conference, 1992. PESC '92 Record.*, volume 1, pp.708–713.

[17] **Hou, C.L.**, **Wu, J.**, **Zhang, M.**, **ming Yang, J. and Li, J.P.** (2004). Application of adaptive algorithm of solar cell battery charger, *IEEE International Conference on Electric Utility Deregulation, Restructuring and Power Technologies, 2004. (DRPT 2004).*, volume 2, pp.810–813.

[18] **El-Shibini, M. and Rakha, H.** (1989). Maximum power point tracking technique, *Electrotechnical Conference, 1989. Proceedings.'Integrating Research, Industry and Education in Energy and Communication Engineering', MELECON'89., Mediterranean*, IEEE, pp.21–24.

[19] **Pan, C.T.**, **Chen, J.Y.**, **Chu, C.P. and Huang, Y.S.** (1999). A fast maximum power point tracker for photovoltaic power systems, *The 25th Annual Conference of the IEEE Industrial Electronics Society, 1999. IECON '99 Proceedings.*, volume 1, pp.390–393.

[20] **Takashima, T.**, **Tanaka, T.**, **Amano, M. and Ando, Y.** (2000). Maximum output control of photovoltaic (PV) array, *(IECEC) 35th Intersociety Energy Conversion Engineering Conference and Exhibit, 2000.*, volume 1, pp.380–383.

[21] **Solodovnik, E.**, **Liu, S. and Dougal, R.** (2004). Power controller design for maximum power tracking in solar installations, *IEEE Transactions on Power Electronics*, ***19***(5), pp.1295–1304.

[22] **de Carvalho, P.**, **Pontes, R.**, **Oliveira, D.S., J.**, **Riffel, D.**, **de Oliveira, R. and Mesquita, S.** (2004). Control method of a photovoltaic powered reverse osmosis plant without batteries based on maximum power point tracking, *IEEE/PES Transmission and Distribution Conference and Exposition: Latin America, 2004*, pp.137–142.

[23] **Rivera ritz, E. and Peng, F.** (2004). A novel method to estimate the maximum power for a photovoltaic inverter system, *IEEE 35th Annual Power Electronics Specialists Conference, 2004. PESC 04. 2004*, volume 3, pp.2065–2069.

[24] **Zhang, M.**, **Wu, J. and Zhao, H.** (2004). The application of slide technology in PV maximum power point tracking system, *Fifth World Congress on Intelligent Control and Automation, 2004. WCICA 2004.*, volume 6, pp.5591–5594.

[25] **Castaner, L. and Silvestre, S.** (2002). *Modelling photovoltaic systems using PSpice*, John Wiley and Sons.

[26] **I.H., A. and A.M., S.** (2000). Array simulation model for Matlab-Simulink GUI Environment, *European Photovoltaic Solar Energy Conference*.

[27] **Green, M.A.** (2003). General temperature dependence of solar cell performance and implications for device modelling, *Progress in Photovoltaics: Research and Applications*, ***11***(5), pp.333–340.

[28] **Soto, W.D.**, **Klein, S. and Beckman, W.** (2006"). Improvement and validation of a model for photovoltaic array performance, *Solar Energy*, ***80***(1), pp.78 – 88.

[29] **Skoplaki, E. and Palyvos, J.** (2009). Operating temperature of photovoltaic modules: A survey of pertinent correlations, *Renewable Energy*, ***34***(1), pp.23 – 29.

APPENDICES

APPENDIX A.1

```
//header*********************************************************************************
include <stdlib.h> //header for pso
include <math.h> //header for pso
include <mega32.h> //header for atmega32
include <io.h> //header for atmega32
include <delay.h> //header for delay
include <stdio.h> //header for rand
//Global parameters ***********************************************************************
int lowerbound=0; //lowebound for
variables
int upperbound=100; //upper bound for
variables
int velocitylowerbound;
int velocityupperbound;
int bestcost[3]; iterationsbestcost
int particleposition[5]; 5 is number of npop
int particlevelocity[5];
int particlecost[5];
int particlebestposition[5];
int particlebestcost[5];
int globalbestcost=0;
//definition of problem *******************************************************************
int watt()
{
int x,y,m,n;
DDRD = 0xFF;
DDRB=0xFF;
DDRA=0;
ADCSRA=0x87;
ADMUX=0xC0;
ADCSRA|=(1 ≪ ADSC);
while((ADCSRA&(1 ≪ ADIF)) == 0);
{x = ADCL;
y = ADCH;
y = (y ≪ 8);
y = y + x;
y = (y*20);
}
ADCSRA = 0x87;
ADMUX = 0xC1;
{ADCSRA| = (1 << ADSC);
{while((ADCSRA&(1 << ADIF)) == 0);
m = ADCL;
```

```
n = ADCH;
n = (n << 8);
n = n + m;
n = (n*10); //becauseofvoltagedivider
n = ((n − 1000)*10); //(2.5//0025) = 1000
y = (n*0.0025*y); //becausewedividethevaluestwotimeoneincurrentandothervoltage
}
}
return y;
}
//definitionofpwm∗∗∗∗∗∗∗∗∗∗∗∗∗∗∗∗∗∗∗∗∗∗∗∗∗∗∗∗∗∗∗∗∗∗∗∗∗∗∗∗
voidpwm()
{
DDRD| = (1 << 5);
ICR1H = 0x00;
ICR1L = 99;
OCR1AH = 0x00;
TCCR1A = 0x82;
TCCR1B = 0x19;
}
//definition of a function which produce numbers between two boundary∗∗∗∗∗∗∗∗
intatma()
{
inta = rand()     //(upperbound − lowerbound + 1) + lowerbound;
return a;
}}
//parameters∗∗∗∗∗∗∗∗∗∗∗∗∗∗∗∗∗∗∗∗∗∗∗∗∗∗∗∗∗∗∗∗∗∗∗∗∗∗∗∗∗∗∗∗
int velocityupperbound, velocitylowerbound, w, c1, c2, it, i, globalbestposition,
npop = 5, itmax = 3, wdamp = .9;
//main∗∗∗∗∗∗∗∗∗∗∗∗∗∗∗∗∗∗∗∗∗∗∗∗∗∗∗∗∗∗∗∗∗∗∗∗∗∗∗∗∗∗∗∗∗∗∗∗
voidmain()
{{
//Constriction Coefficients
w = 1;
c1 = 1;
c2 = 2;
//initializition∗∗∗∗∗∗∗∗∗∗∗∗∗∗∗∗∗∗∗∗∗∗∗∗∗∗∗∗∗∗∗∗∗∗∗∗∗∗∗∗∗∗
pso :
globalbestcost = 0;
velocityupperbound = ((.1) ∗ (upperbound − lowerbound));
velocitylowerbound = −velocityupperbound;
for(i = 1; i < npop; i++)
{{
//initilizeposition
particleposition[i] = atma();
//initializeparticlevelocity
particlevelocity[i] = 0;
//evaluation
OCR1AL = particleposition[i];
```

```
pwm();
delay_ms(10);
particlecost[i] = watt();
//updatepersonalbest
particlebestposition[i] = particleposition[i];
particlebestcost[i] = particlecost[i];
//updateglobalbest
if(particlebestcost[i] > globalbestcost)
{globalbestposition = particlebestposition[i]; globalbestcost = particlebestcost[i];}

//pso main loop*******************************************
for(it = 0; it < itmax; it++)
{
for(i = 1; i < npop; i++)
{
//updatevelocity
particlevelocity[i] = (w*particlevelocity[i]) + ((c1*(atma())*.01)*((particlebestposition[i] −
particleposition[i]))) + (((c2*atma()*.01)*(globalbestposition −
particleposition[i])));
//applyvelocitylimit
if(particlevelocity[i] > velocityupperbound)
{particlevelocity[i] = velocityupperbound;}
if(particlevelocity[i] < velocitylowerbound)
{particlevelocity[i] = velocitylowerbound;}
//updateposition
particleposition[i] = particleposition[i] + particlevelocity[i];
//applypositionlimit
if(particleposition[i] > upperbound)
{particleposition[i] = upperbound;}
if(particleposition[i] < lowerbound)
{particleposition[i] = lowerbound;}
//evaluation
OCR1AL = particleposition[i];
pwm();
delay_ms(10);
particlecost[i] = watt();
//updatepersonalbest
if(particlecost[i] > particlebestcost[i])
{particlebestcost[i] = particlecost[i];
particlebestposition[i] = particleposition[i];
//updateglobalbest
if(particlebestcost[i] > globalbestcost)
{globalbestposition = particlebestposition[i];
globalbestcost = particlebestcost[i];}}
}
bestcost[it] = globalbestcost;
w = w*wdamp;
}
OCR1AL = globalbestposition;
```

```
//delay_ms(1);
pwm();
delay_ms(1000);
goto pso;}
```

APPENDIX B.Datasheets

2.1 Solar panel Datasheet

SUNPOWER

A-300 SOLAR CELL
MONO CRYSTALLINE SILICON

Physical Characteristics

Construction:	All-back contact
Dimensions:	125 mm x 125 mm - nominal
Thickness:	270 μm ± 40 μm

ELECTRICAL CHARACTERISTICS OF TYPICAL CELL AT STANDARD TEST CONDITIONS (STC)

STC is defined as: irradiance of 1000W/m^2, spectrum AM 1.5g and cell temperature of 25°C

Open Circuit Voltage:	0.670 V
Short Circuit Current:	5.9 A
Maximum Power Voltage:	0.560 V
Maximum Power Current:	5.54 A
Rated Power:	3.1 W
Efficiency:	Up to 21.5 %

Temperature Coefficients

Voltage:	-1.9 mV / °C
Power:	-0.38 % / °C

ATTRIBUTES

- High efficiency reduces module assembly and system installation costs
- Uniform front appearance - no contact grid
- Back contact design simplifies circuit assembly
- Lower temperature coefficient improves energy delivery

PACKAGING

- Cells are packed in boxes of 1000 each; grouped in shrink-wrapped stacks of 50 with interleaving
- Twelve boxes are packed in a water-resistant "Master Carton" containing 12,000 cells suitable for air transportation

A-300 CELL PERFORMANCE - TYPICAL I-V CURVE

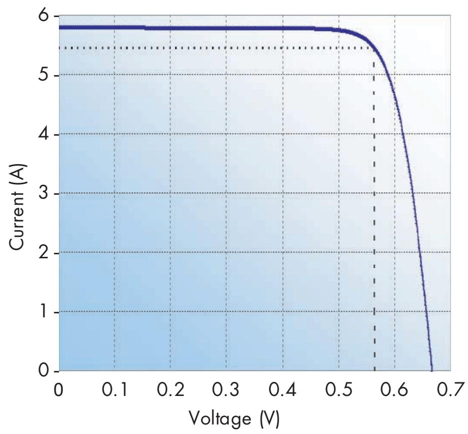

CELL BACKSIDE VIEW
(Dimensions in mm)

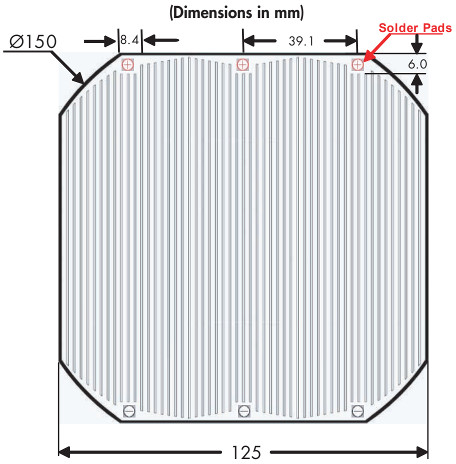

Document#: 70-0006 Rev04

SunPower Corporation®
1.877.786.0123 Email: sales@sunpowercorp.com www.sunpowercorp.com
A Subsidiary of Cypress Semiconductor

2.2 MOSFET Datasheet

International
IOR Rectifier

PD-9.441D

IRFP150

HEXFET® Power MOSFET

- Dynamic dv/dt Rating
- Repetitive Avalanche Rated
- Isolated Central Mounting Hole
- 175°C Operating Temperature
- Fast Switching
- Ease of Paralleling
- Simple Drive Requirements

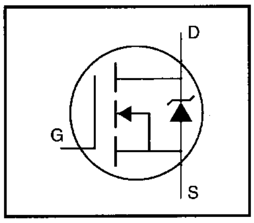

V_{DSS} = 100V

$R_{DS(on)}$ = 0.055Ω

I_D = 41A

Description

Third Generation HEXFETs from International Rectifier provide the designer with the best combination of fast switching, ruggedized device design, low on-resistance and cost-effectiveness.

The TO-247 package is preferred for commercial–industrial applications where higher power levels preclude the use of TO-220 devices. The TO-247 is similar but superior to the earlier TO-218 package because of its isolated mounting hole. It also provides greater creepage distance between pins to meet the requirements of most safety specifications.

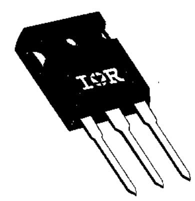

TO-247AC

DATA SHEETS

Absolute Maximum Ratings

	Parameter	Max.	Units
I_D @ T_C = 25°C	Continuous Drain Current, V_{GS} @ 10 V	41	A
I_D @ T_C = 100°C	Continuous Drain Current, V_{GS} @ 10 V	29	
I_{DM}	Pulsed Drain Current ①	160	
P_D @ T_C = 25°C	Power Dissipation	230	W
	Linear Derating Factor	1.5	W/°C
V_{GS}	Gate-to-Source Voltage	±20	V
E_{AS}	Single Pulse Avalanche Energy ②	830	mJ
I_{AR}	Avalanche Current ①	41	A
E_{AR}	Repetitive Avalanche Energy ①	19	mJ
dv/dt	Peak Diode Recovery dv/dt ③	5.5	V/ns
T_J T_{STG}	Operating Junction and Storage Temperature Range	-55 to +175	°C
	Soldering Temperature, for 10 seconds	300 (1.6mm from case)	
	Mounting Torque, 6-32 or M3 screw	10 lbf•in (1.1 N•m)	

Thermal Resistance

	Parameter	Min.	Typ.	Max.	Units
$R_{θJC}$	Junction-to-Case	—	—	0.65	°C/W
$R_{θCS}$	Case-to-Sink, Flat, Greased Surface	—	0.24	—	
$R_{θJA}$	Junction-to-Ambient	—	—	40	

947

2.3 Diode Datasheet

MUR805G, MUR810G, MUR815G, MUR820G, MUR840G, MUR860G, MURF860G, SUR8820G, SUR8840G

ON Semiconductor®

http://onsemi.com

Switch-mode Power Rectifiers

This series is designed for use in switching power supplies, inverters and as free wheeling diodes.

Features

- Ultrafast 25 and 50 Nanosecond Recovery Time
- 175°C Operating Junction Temperature
- Epoxy Meets UL 94 V−0 @ 0.125 in
- Low Forward Voltage
- Low Leakage Current
- Reverse Voltage to 600 V
- ESD Ratings:
  - Machine Model = C (> 400 V)
  - Human Body Model = 3B (> 16,000 V)
- SUR8 Prefix for Automotive and Other Applications Requiring Unique Site and Control Change Requirements; AEC−Q101 Qualified and PPAP Capable
- These Devices are Pb−Free and are RoHS Compliant*

Mechanical Characteristics:

- Case: Epoxy, Molded
- Weight: 1.9 Grams (Approximately)
- Finish: All External Surfaces Corrosion Resistant and Terminal Leads are Readily Solderable
- Lead Temperature for Soldering Purposes: 260°C Max for 10 Seconds

ULTRAFAST RECTIFIERS
8.0 AMPERES, 50−600 VOLTS

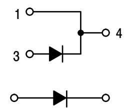

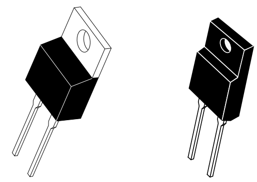

TO−220AC
CASE 221B
STYLE 1

TO−220 FULLPAK
CASE 221AG
STYLE 1

MARKING DIAGRAMS

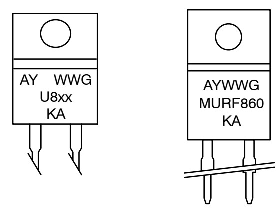

A = Assembly Location
Y = Year
WW = Work Week
U8XX = Device Code
xx = 05, 10, 15, 20, 40, or 60
G = Pb−Free Package
KA = Diode Polarity

ORDERING INFORMATION

See detailed ordering and shipping information in the package dimensions section on page 7 of this data sheet.

*For additional information on our Pb−Free strategy and soldering details, please download the ON Semiconductor Soldering and Mounting Techniques Reference Manual, SOLDERRM/D.

February, 2014 − Rev. 13

Publication Order Number:
MUR820/D

2.4 Microcontroller Datasheet

Features

- High-performance, Low-power Atmel®AVR® 8-bit Microcontroller
- Advanced RISC Architecture
  - 131 Powerful Instructions – Most Single-clock Cycle Execution
  - 32 × 8 General Purpose Working Registers
  - Fully Static Operation
  - Up to 16 MIPS Throughput at 16MHz
  - On-chip 2-cycle Multiplier
- High Endurance Non-volatile Memory segments
  - 32Kbytes of In-System Self-programmable Flash program memory
  - 1024Bytes EEPROM
  - 2Kbytes Internal SRAM
  - Write/Erase Cycles: 10,000 Flash/100,000 EEPROM
  - Data retention: 20 years at 85°C/100 years at 25°C(1)
  - Optional Boot Code Section with Independent Lock Bits
    In-System Programming by On-chip Boot Program
    True Read-While-Write Operation
  - Programming Lock for Software Security
- JTAG (IEEE std. 1149.1 Compliant) Interface
  - Boundary-scan Capabilities According to the JTAG Standard
  - Extensive On-chip Debug Support
  - Programming of Flash, EEPROM, Fuses, and Lock Bits through the JTAG Interface
- Peripheral Features
  - Two 8-bit Timer/Counters with Separate Prescalers and Compare Modes
  - One 16-bit Timer/Counter with Separate Prescaler, Compare Mode, and Capture Mode
  - Real Time Counter with Separate Oscillator
  - Four PWM Channels
  - 8-channel, 10-bit ADC
    8 Single-ended Channels
    7 Differential Channels in TQFP Package Only
    2 Differential Channels with Programmable Gain at 1x, 10x, or 200x
  - Byte-oriented Two-wire Serial Interface
  - Programmable Serial USART
  - Master/Slave SPI Serial Interface
  - Programmable Watchdog Timer with Separate On-chip Oscillator
  - On-chip Analog Comparator
- Special Microcontroller Features
  - Power-on Reset and Programmable Brown-out Detection
  - Internal Calibrated RC Oscillator
  - External and Internal Interrupt Sources
  - Six Sleep Modes: Idle, ADC Noise Reduction, Power-save, Power-down, Standby and Extended Standby
- I/O and Packages
  - 32 Programmable I/O Lines
  - 40-pin PDIP, 44-lead TQFP, and 44-pad QFN/MLF
- Operating Voltages
  - 2.7V - 5.5V for ATmega32L
  - 4.5V - 5.5V for ATmega32
- Speed Grades
  - 0 - 8MHz for ATmega32L
  - 0 - 16MHz for ATmega32
- Power Consumption at 1MHz, 3V, 25°C
  - Active: 1.1mA
  - Idle Mode: 0.35mA
  - Power-down Mode: < 1µA

8-bit AVR® Microcontroller with 32KBytes In-System Programmable Flash

ATmega32
ATmega32L

2503Q–AVR–02/11

2.5 MOSFET Driver Datasheet

TOSHIBA Photocoupler GaAℓAs Ired & Photo−IC

TLP250

Transistor Inverter
Inverter For Air Conditioner
IGBT Gate Drive
Power MOS FET Gate Drive

Unit in mm

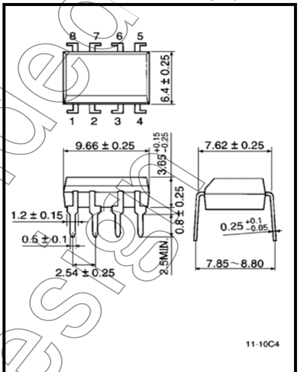

TOSHIBA 11−10C4
Weight: 0.54 g (typ.)

The TOSHIBA TLP250 consists of a GaAlAs light emitting diode and a integrated photodetector.
This unit is 8−lead DIP package.
TLP250 is suitable for gate driving circuit of IGBT or power MOS FET.

- Input threshold current: I_F=5mA(max.)
- Supply current (I_{CC}): 11mA(max.)
- Supply voltage (V_{CC}): 10−35V
- Output current (I_O): ±1.5A (max.)
- Switching time (t_{pLH}/t_{pHL}): 0.5μs(max.)
- Isolation voltage: 2500V_{rms}(min.)
- UL recognized: UL1577, file No.E67349
- Option(D4)
  VDE Approved : DIN EN60747-5-2
  Maximum Operating Insulation Voltage : 890V_{PK}
  Highest Permissible Over Voltage : 4000V_{PK}

**(Note):When a EN60747-5-2 approved type is needed,
Please designate "Option(D4)"**

Pin Configuration (top view)

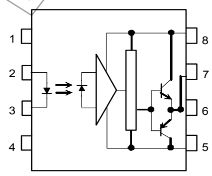

1 : N.C.
2 : Anode
3 : Cathode
4 : N.C.
5 : GND
6 : V_O (Output)
7 : V_O
8 : V_{CC}

Truth Table

		Tr1	Tr2
Input LED	On	On	Off
	Off	Off	On

Schmatic

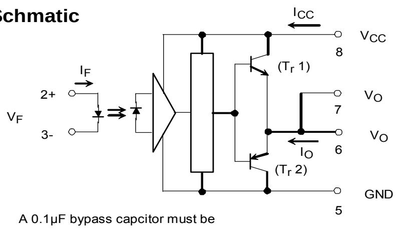

A 0.1μF bypass capcitor must be connected between pin 8 and 5 (See Note 5).

2.6 Current Sensor Datasheet

Current Transducer LTS 25-NP

I_{PN} = 25 At

For the electronic measurement of currents: DC, AC, pulsed, mixed with galvanic isolation between the primary circuit (high power) and the secondary circuit (electronic circuit).

16054

Electrical data

I_{PN}	Primary nominal current rms		25	At
I_{PM}	Primary current, measuring range		0 .. ± 80	At
V_{OUT}	Output voltage (Analog) @ I_P		2.5 ± (0.625·I_P/I_{PN})	V
	I_P = 0		2.5 [1]	V
G	Sensitivity		25	mV/A
N_S	Number of secondary turns (± 0.1 %)		2000	
R_L	Load resistance		≥ 2	kΩ
R_{IM}	Internal measuring resistance (± 0.5 %)		50	Ω
TCR_{IM}	Temperature coefficient of R_{IM}		< 50	ppm/K
V_C	Supply voltage (± 5 %)		5	V
I_C	Current consumption @ V_C = 5 V	Typ	28+I_S[2]+(V_{OUT}/R_L)	mA

Accuracy - Dynamic performance data

X	Accuracy @ I_{PN}, T_A = 25°C		± 0.2		%
	Accuracy with R_{IM} @ I_{PN}, T_A = 25°C		± 0.7		%
ε_L	Linearity error		< 0.1		%
			Typ	Max	
TCV_{OUT}	Temperature coefficient of V_{OUT} @ I_P = 0	- 10°C .. + 85°C	50	100	ppm/K
		- 40°C .. - 10°C		150	ppm/K
TCG	Temperature coefficient of G	- 40°C .. + 85°C		50 [3]	ppm/K
V_{OM}	Magnetic offset voltage @ I_P = 0,				
	after an overload of 3 x I_{PN}			± 0.5	mV
	5 x I_{PN}			± 2.0	mV
	10 x I_{PN}			± 2.0	mV
t_{ra}	Reaction time @ 10 % of I_{PN}		< 100		ns
t_r	Response time to 90 % of I_{PN} step		< 400		ns
di/dt	di/dt accurately followed		> 60		A/µs
BW	Frequency bandwidth (0 .. - 0.5 dB)		DC .. 100		kHz
	(- 0.5.. 1 dB)		DC .. 200		kHz

General data

T_A	Ambient operating temperature	- 40 .. + 85	°C
T_S	Ambient storage temperature	- 40.. + 100	°C
m	Mass	10	g
	Standards	EN 50178: 1997 IEC 60950-1: 2001	

Notes: [1] Absolute value @ T_A = 25°C, 2.475 < V_{OUT} < 2.525
[2] I_S = I_P/N_S
[3] Only due to TCR_{IM}.

Features

- Closed loop (compensated) multi-range current transducer using the Hall effect
- Unipolar voltage supply
- Isolated plastic case recognized according to UL 94-V0
- Compact design for PCB mounting
- Incorporated measuring resistance
- Extended measuring range.

Advantages

- Excellent accuracy
- Very good linearity
- Very low temperature drift
- Optimized response time
- Wide frequency bandwidth
- No insertion losses
- High immunity to external interference
- Current overload capability.

Applications

- AC variable speed drives and servo motor drives
- Static converters for DC motor drives
- Battery supplied applications
- Uninterruptible Power Supplies (UPS)
- Switched Mode Power Supplies (SMPS)
- Power supplies for welding applications.

Application domain

- Industrial.

CURRICULUM VITAE

Name Surname: Mohammadreza Esmali Nojehdeh

Place and Date of Birth: Ardebil-Iran 1987

Adress: No93-Azerbayjan Avenue-Ardebil-Ardebil-Iran

E-Mail:nojehdeh@itu.edu.tr

B.Sc.: Islamic Azad University